Multilayer assembly of phase change material and bio-based concrete: A passive envelope to improve the energy and hygrothermal performance of buildings

Dongxia Wu, Mourad Rahim, Mohammed El Ganaoui, Rachid Bennacer, Bin Liu

To cite this version:

Dongxia Wu, Mourad Rahim, Mohammed El Ganaoui, Rachid Bennacer, Bin Liu. Multilayer assembly of phase change material and bio-based concrete: A passive envelope to improve the energy and hygrothermal performance of buildings. Energy Conversion and Management, 2022, 257, pp.115454. 10.1016/j.enconman.2022.115454 . hal-04274351

HAL Id: hal-04274351
https://cnrs.hal.science/hal-04274351

Submitted on 22 Jul 2024

Version of Record: https://www.sciencedirect.com/science/article/pii/S0196890422002503
Manuscript_fcdc1acf5356a0c7395abafd5ac3c465

Multilayer assembly of phase change material and bio-based concrete: A passive envelope to improve the energy and hygrothermal performance of buildings

Dongxia Wu[a,*]; Mourad Rahim[a]; Mohammed El Ganaoui [a,**]; Rachid Bennacer[b]; Bin Liu[c]

a. University of Lorraine, LERMAB, IUT H Poincaré de Longwy, 168 Rue de Lorraine. Cosnes et Romain, 54400 Longwy, France

b. University of Paris-Saclay, ENS Paris-Saclay, CNRS, LMT -, 91190, Gif-sur-Yvette, France

c. Tianjin Key Laboratory of Refrigeration Technology, Tianjin University of Commerce, Tianjin 300134, China

[*]Corresponding author[**] The two authors have the same contribution to this study.

Tel: +33-0781968839; E-mail: dongxia.wu@univ-lorraine.fr (Dongxia Wu);

Tel: +33-0664947141; E-mail: mohammed.el-ganaoui@univ-lorraine.fr (Mohammed El Ganaoui).

Address: IUT Henri Poincaré de Longwy. 168 Rue de Lorraine. Cosnes et Romain, 54400 Longwy, France

Abstract

Phase change materials (PCMs) can improve indoor thermal comfort and reduce energy consumption, while bio-based concrete is an environment-friendly material that enables indoor humidity regulation and heat insulation. However, only a few studies have explored the integrated application of the two materials and comprehensively analyzed the energy and hygrothermal performance. In this study, a passive envelope solution that integrates PCM and hemp concrete is proposed to improve buildings' energy, thermal, and hygric performances simultaneously. Four integrated scenarios were considered and compared with a baseline scenario (hemp concrete only). The performance of the integrated envelope was studied numerically based on the impact of the PCM's properties and its location in the envelope. The results highlight the indispensable role moisture transfer plays in determining the indoor hygric environment and heat load, as well as the valuable effect of the integrated envelope on improving both energy and hygrothermal performance. Scenario 4/5 (with PCM closest to the interior) in the summer showed the greatest performance improvement compared to the baseline scenario, with reductions of 8.2%, 46.3%, and 43.7% for heat load, temperature fluctuation, and partial water vapor pressure fluctuation, respectively. The impact of the PCM properties in scenario 4/5 illustrate that the optimization of the integrated envelope can be achieved by increasing the thickness and latent heat of the PCM and identifying its appropriate phase transition range. From a year-round perspective, scenario 4/5 is also notable, as it shows great potential for saving energy and adapting to climate humidity variation while guaranteeing moisture equilibrium within the hemp concrete. The three-year assessment confirmed a lack of condensation and no risk of mold growth for such an integrated envelope, as the relative humidity in key locations remains below 75%.

Keywords

Phase change material (PCM); Bio-based concrete; Passive building envelope; Heat and moisture transfer; Hygrothermal performance; Energy savings

Nomenclature

C	specific heat capacity (J/(kg·K))
C^*	effective heat capacity of PCM (J/(kg·K))
F_{sky}	radiation view factor from sky to the envelope
h_t	convective heat transfer coefficient $(\mathrm{W/(m^2 \cdot K)})$
h_m	convective mass transfer coefficient $(\mathrm{kg/(m^2 \cdot s \cdot Pa)})$
I_{rad}	solar radiation on exterior surface $(\mathrm{W/m^2})$
j	total moisture flux $(\mathrm{kg/(m^2. s)})$
j_l	liquid moisture flux $(\mathrm{kg/(m^2 \cdot s)})$
j_v	vapor moisture flux $(\mathrm{kg/(m^2 \cdot s)})$
J	moisture load $(\mathrm{kg/m^2})$
K_w	liquid water permeability (kg/(Pa·m·s))
L_v	latent heat of evaporation (J/kg)
Le	Lewis number
M_w	molar mass of water (kg/mol)
p_v	partial water vapor pressure (Pa)
$p_{v,sat}$	saturation vapor pressure (Pa)
p_c	capillary pressure (Pa)
q	heat flux $(\mathrm{W/m^2})$
Q	heat load $(\mathrm{W \cdot h/m^2})$
R	universal gas constant (J/(kg·K))
T	temperature (°C)
w	volumetric moisture content $(\mathrm{kg/m^3})$

Greek symbols

α	solar absorptivity on exterior surface
δ_p	water vapor permeability $(\mathrm{kg/(Pa \cdot m \cdot s)})$
ε	infrared emittance of the exterior wall surface
θ	relative error
ξ	sorption capacity
ρ	density $(\mathrm{kg/m^3})$
σ	Stefan-Boltzmann constant $(\mathrm{W/(m^2 \cdot K^4)})$
λ	thermal conductivity $(\mathrm{W/(m \cdot K)})$
λ^*	effective thermal conductivity of PCM $(\mathrm{W/(m \cdot K)})$
φ	relative humidity (%)

Subscripts

a	air
amp	amplitude
$crit$	critical
e	exterior
hc	hemp concrete
i	interior
pcm	PCM
$peak$	peak value
sky	sky
v	moisture vapor

$valley$	valley value
w	water
$x = 0$	exterior surface of envelope
$x = l$	interior surface of envelope

1. Introduction

Energy consumption and CO_2 emissions from the building industry account for 35% and 38% of total energy consumption and emissions, respectively [1]. Building envelopes, as an important part of buildings, are responsible for more than half (51%) of total building energy consumption [2]. In addition, envelopes are the medium for indoor–outdoor environmental transmission, playing an important role in regulating indoor temperature and relative humidity. Therefore, innovation in building envelopes plays a crucial role in saving energy, reducing emissions, and regulating the indoor environment.

Phase change material (PCM) has been extensively applied to building envelopes because of its considerable heat storage capacity (thermal inertia) [3]. PCMs have been widely studied in different cities and climates [4] as part of building construction (e.g., envelopes [5], floors [6], ceilings [7], and windows [8]) in order to improve thermal comfort and save building energy [9]. However, the thermal performance of PCM varies with different properties and location in the building structure. Lee [10] found that the thermal performance of PCM was different at the same location in the south and west walls of the building being investigated. Li [11] reported that the heat transfer reduction was different when the PCM was placed on the exterior and interior sides. Yu [12] studied the performance of PCMs with different phase transition ranges in five climate regions, and the results indicated that the optimal phase transition temperature was low in the mild region and high in the hot summer and cold winter region. Moreover, according to the study [13], the heat flux fluctuation decreases with increasing PCM thickness and latent heat.

Bio-based concrete has also attracted attention in recent years, as its raw material comes from nature, thus lowering the cost of application [14] and reducing carbon emissions [15]. Furthermore, bio-based concrete is a lightweight thermal insulation material that contributes to indoor thermal comfort and energy efficiency [16]. Moreover, it is an excellent hygroscopic material, with a high moisture buffer capacity (moisture inertia) resulting from its capacity to absorb and desorb moisture from the surrounding environment. Chennouf [17] and Rahim [18] measured and proved the “excellent” moisture buffer capacity of date palm cement, flax, straw, and hemp lime concrete samples; they found the moisture buffer capacity of these materials to be greater than that of conventional materials. The hygroscopic behavior has been proven to be highly related to the temperature characteristic. Poyet [19] theoretically explained the relationship between vapor sorption properties and temperature. Chennouf [20], Wu [21], and Colinart [22] experimentally and numerically studied the relationship between temperature and hygric properties and suggested that there is a high coupling between heat and moisture transfer and that the hygric properties are more susceptible to temperature.

Consequently, it is valuable to integrate the thermal inertia of PCMs with the moisture inertia of hygroscopic materials, making it possible to improve the energy, thermal, and hygric performance of the envelope simultaneously. However, when it comes to the integration of these two types of materials, most studies have focused only on their thermal and energy performance while neglecting their hygric performance. Therefore, to date, only a few studies have focused on both the thermal and hygric performances of integrated materials, and these studies generally fall into two categories. The first category deals with the mixed sample integration and preparation of PCMs and hygroscopic materials (zeolite [23], sepiolite [24], gypsum [25], metal-organic frameworks[26], diatomite [27], etc.) as well as the measurement and analysis of the properties (morphological, thermal, hygroscopic, chemical, etc.) of the integrated samples. The second category focuses on the application of the integrated materials. Fraine [28] found that a phase change humidity control material that incorporates microencapsulated PCM and diatomite can reduce fluctuations in temperature and relative humidity on the interior surface. Similar results were also found in [29], which integrated macro-encapsulated PCM and concrete walls. By assessing their water content, Park [30] and Chang [31] proved that a PCM–gypsum composite and a PCM–wood composite improved hygrothermal performance. Wu [32] assessed the hygrothermal and energy performance of a building that used PCM and diatomite as envelopes, and the results demonstrated the ability to regulate temperature and humidity.

These two categories are of great interest from the perspective of sample characterization and basic hygrothermal behavior assessment. However, an overall analysis of energy performance (total, sensible, and latent heat load) and the quantification of hygric performance are also important. Moreover, because of the coupling between heat and moisture transfer, it is necessary to study the thermal, hygric, and energy performances comprehensively. First, the principle that PCMs affect the hygric performance of the envelope by influencing its thermal performance needs to be investigated. Further, the effect of hygroscopic materials on hygric and energy performance is also worth studying. In addition, considering that the location and properties of the PCM affect the temperature distribution in the envelope, it is meaningful to explore the optimization strategy by studying the impact of PCM parameters on the performance of the integrated envelope. However, among similar studies (in the second category mentioned above), few focus on performance optimization. Although some studies [28, 29] have analyzed the impact of PCM location, they focused only on temperature and relative humidity behavior and did not investigate energy performance.

In this paper, a multilayered passive building envelope is proposed by integrating PCM and bio-based concrete, namely hemp concrete (HC). Four scenarios in which PCM was placed in different locations were considered in comparison to a baseline scenario (HC only). Rome, with its Mediterranean climate, was chosen as a climatic environment where PCM is easily activated and utilized [33]. The objectives of this study are to prove the importance of moisture transfer, to identify the impact of PCM location and properties (thickness, latent heat, and phase transition range) on the energy and hygrothermal performance of the integrated envelope, and to assess performance and application risk. The main contributions are as follows: (1) establishing and validating a multilayer envelope model that couples heat and moisture transfer; (2) analyzing the relationship between energy, thermal, and hygric performance, proving the importance of moisture transfer; (3) investigating the impact of PCM, its location, and its properties on performance; (4) assessing annual energy and hygric performance; and (5) assessing the risk of condensation and mold growth over a three-year period.

2. Multilayer envelope description and mathematical model

2.1 Multilayer envelope description

Fig. 1 shows five envelope scenarios, including one baseline scenario with HC only and four integrated scenarios with PCM at different locations. For the integrated scenarios, the HC layer was assumed to be divided into four uniform parts by three gaps along the thickness direction, and PCMs were inserted into the gaps; the resulting scenarios were named scenario 2/5, 3/5, and 4/5, respectively. The scenario with PCM on the outermost layer was named scenario 1/5. The thickness of the baseline scenario was 25 cm. The integrated scenarios comprised a 24-cm HC layer and a 1-cm PCM layer. The distance between the PCM and the interior surface in scenario 4/5 was 6 cm, which was thicker than the penetration depth of the HC [34].

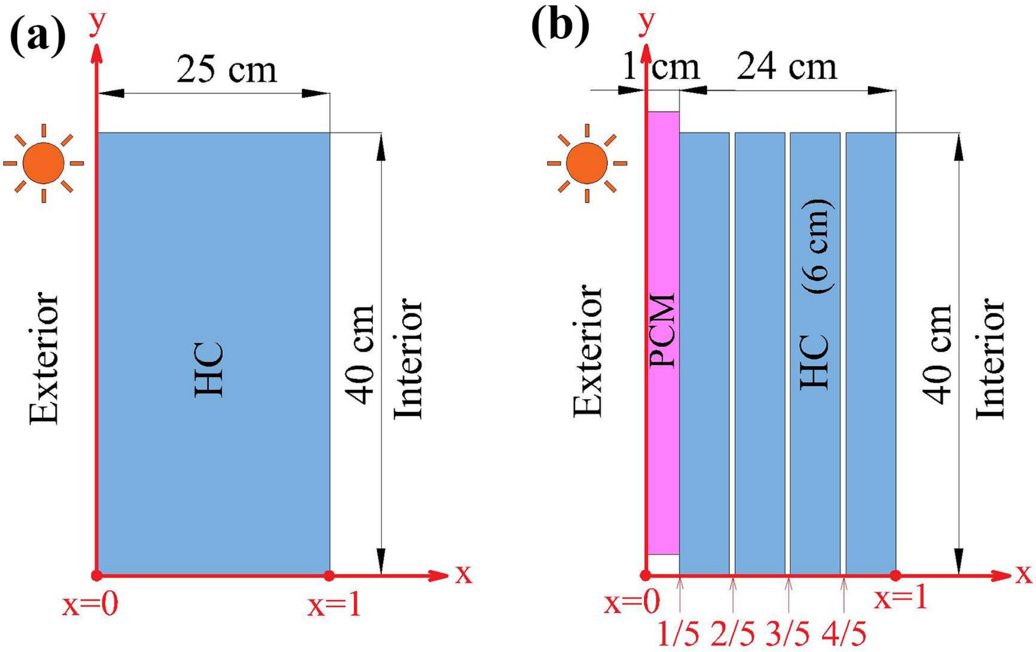

Fig. 1. Two-dimensional layout of envelope: (a) baseline scenario and (b) integrated scenario

The HC is composed of hemp shives (64%), water (24%), and a lime-based binder (12%). The PCM is a finished hydrocarbon-based PCM [35] comprised of an ethylene-based polymer (40%) and paraffin wax (60%), with a 0.1 mm aluminum sheet laminated on both sides. Their physical properties are shown in Table 1. To study the effect of PCM properties on performance, three additional phase transition ranges (16–20, 20–24, and 28–32 °C), three additional latent heats (62.9, 117.8, and 145.3 kJ/(kg·K)), and two additional thicknesses (0.02 and 0.03 m) were considered. The specific heat capacities and thermal conductivities of these PCMs are presented in Fig. 2 (a) and (b).

	HC[a]	PCM
Density ($\mathrm{kg/m^3}$)	478	810
Specific heat capacity ($\mathrm{kJ/(kg{\cdot}K)}$)	$1.08 + 8.8 \times 10^{-3} w$	Fig. 2 (a)
Thermal conductivity ($\mathrm{W/(m{\cdot}K)}$)	$0.125 + 3.36 \times 10^{-4} w$	Fig. 2 (b)
Latent heat ($\mathrm{kJ/kg}$)	—	90.4
Phase transition range (℃)	—	24–28
Water vapor permeability ($\mathrm{kg/(Pa{\cdot}m{\cdot}s)}$)	$1.26 \times 10^{-11} \times \exp(2.26\varphi)$	—
Volumetric moisture content ($\mathrm{kg/m^3}$)	$\frac{\varphi}{-0.08\varphi^2 + 0.06\varphi + 0.03} - (0.4 - 0.26\varphi)(T - 23)$	—

[a] In the expression of the physical properties of HC, w, φ, and T are the volumetric moisture content, relative humidity (expressed in decimal form), and temperature, respectively.

Table 1 Physical properties of HC [36] and PCM

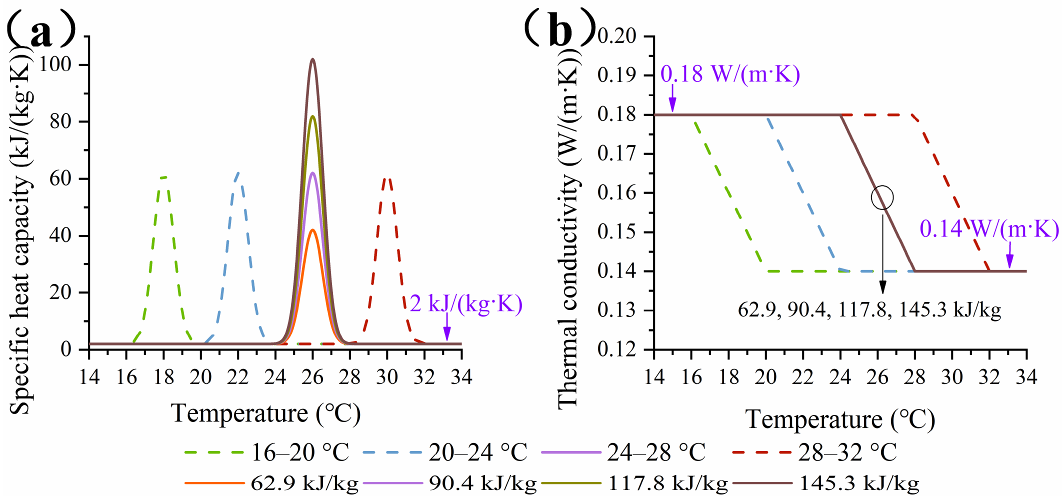

Fig. 2. Thermal properties of PCMs with different phase transition ranges and latent heats: (a) specific heat capacity; (b) thermal conductivity

2.2 Coupled heat and moisture transfer model of HC

Before presenting the mathematical model, the following assumptions are considered:

1) Every element and layer of the envelope is non-deformable, homogeneous, and isotropic.
2) Thermal resistance on the interface between the layers is neglected.
3) Radiative heat transfer between the interior and the envelope is neglected.
4) The air in the pores of the porous structure of the HC is considered an ideal gas.
5) No heat or moisture sources exist in the envelope.
6) A local thermodynamic equilibrium exists between heat and moisture in the envelope.

2.2.1 Moisture transfer

In the model presented, relative humidity (φ) and temperature (T) are chosen as driving potentials of moisture and heat transfer, respectively. The total moisture transfer in porous materials includes vapor diffusion and liquid transport, which follow Fick's law [37] and Darcy's law [38], respectively. The total moisture flux and mass conservation equation [39] can be written as

$$j = j_v + j_l = -\delta_p \nabla p_v - K_w \nabla p_c \tag{1}$$

$$\frac{\partial w}{\partial t} = -\nabla j \tag{2}$$

where j, j_v, and j_l are the total, vapor, and liquid moisture fluxes, respectively; δ_p is the water vapor permeability; p_v is the partial water vapor pressure; K_w is the liquid water permeability; p_c is the capillary pressure; w is the volumetric moisture content.

The sorption moisture retention curve is dependent on both relative humidity and temperature [40]:

$$\frac{\partial w}{\partial t} = \left.\frac{\partial w}{\partial \varphi}\right|_T \frac{\partial \varphi}{\partial t} + \left.\frac{\partial w}{\partial T}\right|_\varphi \frac{\partial T}{\partial t} = \xi_\varphi \frac{\partial \varphi}{\partial t} + \xi_T \frac{\partial T}{\partial t} \tag{3}$$

where ξ is the sorption capacity.

The partial water vapor pressure can be expressed in terms of relative humidity and saturation pressure ($p_{v,sat}$) [41]:

$$p_v = \varphi p_{v,sat} \tag{4}$$

$$p_{v,sat} = 610.5 exp(\frac{17.269T}{237.3+T}) \tag{5}$$

$$\nabla p_v = \nabla(\varphi p_{v,sat}) = \varphi \nabla p_{v,sat} + p_{v,sat} \nabla \varphi = \varphi \frac{dp_{v,sat}}{dT} \nabla T + p_{v,sat} \nabla \varphi \tag{6}$$

The capillary pressure is calculated using the Kelvin equation [42]:

$$p_c = \frac{\rho_w RT}{M_w} ln(\varphi) \tag{7}$$

$$\nabla p_c = \frac{\rho_w R}{M_w} ln(\varphi) \nabla T + \frac{\rho_w RT}{M_w \varphi} \nabla \varphi \tag{8}$$

where ρ_w is the density of water; R is the universal gas constant; M_w is the molar mass of water.

Therefore, the mass conservation equation can be obtained by combining Eqs. (1) – (3).

$$\xi_\varphi \frac{\partial \varphi}{\partial t} + \xi_T \frac{\partial T}{\partial t} = \nabla \left((\delta_p p_{v,sat} + K_w \frac{\rho_w R T}{\varphi M_w}) \ \nabla \varphi + (\delta_p \varphi \frac{d p_{v,sat}}{dT} + K_w \frac{\rho_w R \ ln(\varphi)}{M_w}) \nabla T \right) \tag{9}$$

Eq. (9) can be simplified as

$$\xi_\varphi \frac{\partial \varphi}{\partial t} + \xi_T \frac{\partial T}{\partial t} = \nabla \big(D_\varphi \nabla \varphi + D_T \nabla T \big) \tag{10}$$

$$D_\varphi = \delta_p p_{v,sat} + K_w \frac{\rho_w R T}{\varphi M_w} \tag{11}$$

$$D_T = \delta_p \varphi \frac{d p_{v,sat}}{dT} + K_w \frac{\rho_w R \ ln(\varphi)}{M_w} \tag{12}$$

The liquid water permeability can be written as [43]:

$$K_w = \frac{\delta_p \varphi M_w p_{v,sat}}{R T \rho_w} \tag{13}$$

2.2.2 Heat transfer

Heat transfer in the HC can be described as a change in enthalpy caused by a change in temperature, and it consists of two parts. First, the heat flux gradient is directly proportional to the temperature gradient and the conductivity as defined by Fourier's law. Second, the heat flux gradient can also be transported by the moisture flux, defined as a source term in the general heat equation [44]. Thus, the energy conservation equation [39] can be expressed by

$$\rho_{hc} C_{hc} \frac{\partial T}{\partial t} = \nabla (\lambda_{hc} \nabla T) - L_v \nabla j_v \tag{14}$$

where ρ_{hc} is the density of HC; C_{hc} is the specific heat capacity of HC; λ_{hc} is the thermal conductivity of HC; L_v is the latent heat of evaporation.

According to Eqs. (1) and (6), Eq. (14) can be expressed as

$$\rho_{hc} C_{hc} \frac{\partial T}{\partial t} = \nabla (\lambda_{hc} \nabla T) + L_v \nabla (\delta_p p_{v,sat} \nabla \varphi + \delta_p \varphi \frac{d p_{v,sat}}{dT} \nabla T) \tag{15}$$

Eq. (15) can be simplified as

$$\rho_{hc} C_{hc} \frac{\partial T}{\partial t} = \nabla(\lambda_{hc} \nabla T) + L_v \nabla\left(D_{\varphi,v} \nabla\varphi + D_{T,v} \nabla T\right) \tag{16}$$

$$D_{\varphi,v} = \delta_p p_{v,sat} \tag{17}$$

$$D_{T,v} = \delta_p \varphi \frac{dp_{v,sat}}{dT} \tag{18}$$

Here, the latent heat of evaporation is a function of temperature [45]:

$$L_v = (2500 - 2.4T) \times 10^3 \tag{19}$$

2.3 Heat transfer model of PCM

The effective heat capacity model [46] was chosen to describe the heat transfer of the PCM. This model deals with heat capacity and thermal conductivity as a function of temperature; their curves are shown in Fig. 2 (a) and (b) in Section 2.1, while their functions are described by Eqs. (A.1) and (A.2) in Appendix A. The heat transfer equation of the PCM can be expressed by

$$\rho_{pcm} C^* \frac{\partial T}{\partial t} = \nabla(\lambda^* \nabla T) \tag{20}$$

where ρ_{pcm} is the density of PCM; C^* is the effective heat capacity of PCM; λ^* is the effective thermal conductivity of PCM.

2.4 Boundary conditions

Since the outermost layer comprised the PCM in scenario 1/5 and HC in the remaining scenarios, the boundary conditions were different on the exterior surface.

When HC is the outermost layer, the moisture and heat transfer boundary conditions on the exterior surface are

$$-\left(D_{\varphi}\nabla\varphi + D_T\nabla T\right)\Big|_{x=0} = h_{m,e}(p_{v,e} - p_{v,x=0}) \tag{21}$$

$$-\left(\lambda_{hc}\nabla T + L_v\left(D_{T,v}\nabla T + D_{\varphi,v}\nabla\varphi\right)\right)\Big|_{x=0} = h_{t,e}(T_e - T_{x=0}) + L_v h_{m,e}\left(p_{v,e} - p_{v,x=0}\right) + \alpha I_{rad} + \varepsilon\sigma\left[\left(1 - F_{sky}\right)\left(T_e^4 - T_{x=0}^4\right) + F_{sky}\left(T_{sky}^4 - T_{x=0}^4\right)\right] \tag{22}$$

When PCM is the outermost layer, no moisture transfer happens on the exterior surface and the boundary conditions are expressed as

$$j|_{x=0} = 0 \tag{23}$$

$$-(\lambda^{*}\nabla T)|_{x=0} = h_{t,e}(T_e - T_{x=0}) + \alpha I_{rad} + \varepsilon\sigma\left[\left(1 - F_{sky}\right)\left(T_e^4 - T_{x=0}^4\right) + F_{sky}\left(T_{sky}^4 - T_{x=0}^4\right)\right] \tag{24}$$

For the interior surface, the moisture and heat transfer boundary conditions remain coincident for all scenarios:

$$-\left(D_{\varphi}\nabla\varphi + D_T\nabla T\right)\Big|_{x=l} = h_{m,i}(p_{v,x=l} - p_{v,i}) \tag{25}$$

$$-\left(\lambda_{hc}\nabla T + L_v\left(D_{T,v}\nabla T + D_{\varphi,v}\nabla\varphi\right)\right)\Big|_{x=l} = h_{t,i}(T_{x=l} - T_i) + L_v h_{m,i}\left(p_{v,x=l} - p_{v,i}\right) \tag{26}$$

where $h_{t,e}$ and $h_{t,i}$ are the convective heat transfer coefficients on the exterior and interior surfaces, assumed to be constant with values of 23.26 and 8.72 $\mathrm{W/(m^2{\cdot}K)}$ [47], respectively; $h_{m,e}$ and $h_{m,i}$ are the convective mass transfer coefficients on the exterior and interior surfaces; $p_{v,e}$ and $p_{v,i}$ are the partial water vapor pressures on the exterior and interior surfaces; $p_{v,x=0}$ and $p_{v,x=l}$ are the partial water vapor pressures on the exterior and interior surfaces; T_e and T_i are the temperatures of exterior and interior; $T_{x=0}$ and $T_{x=l}$ are the temperatures on the exterior and interior surfaces; α is the solar absorptivity, assumed to be 0.8; ε is the infrared emittance, assumed to be 0.8; I_{rad} is the solar radiation; σ is the Stefan-Boltzmann constant; F_{sky} is the radiation view factor from the sky to the envelope, from [48]: $F_{sky} = \beta[0.5(1 + cos\gamma)]$. Here, $\gamma = 90°$ for the vertical envelope; $\beta = \sqrt{0.5(1 + cos\gamma)}$; T_{sky} is the sky temperature, given by [49], $T_{sky} = 0.0552T_e^{1.5}$.

The mass transfer coefficient is related to the heat transfer coefficient using the Lewis relationship [50]:

$$h_m = \frac{h_t}{\rho_a C_a Le} \tag{27}$$

where ρ_a is the density of air; C_a is the specific heat capacity of air; Le is the Lewis number.

3. Methodology

3.1 Climate and interior conditions

Fig. 3 (a) depicts the studied climate in Rome, Italy, which is characterized as a Mediterranean climate (according to the Köppen-Geiger climate classification system [51]: Csa). It is mild but humid in winter, and hot with temperate humidity in summer. The interior temperature was determined according to International Standard ISO 13788-2012 [52], which proposes a simplified approach to determining interior conditions based on climate temperature. Fig. 3 (b) shows the seasonally dependent interior temperature, which was set to 25 and 20 °C in summer and winter, respectively, and to vary linearly between 20 and 25 °C in spring and autumn. The interior relative humidity was taken as 50% throughout the year.

Fig. 3 (c) and (d) show the representative climate variation during one week in summer (August 1 to 7) and in winter (January 10 to 17), respectively, in terms of climate temperature, relative humidity, and sol-air temperature ($\mathrm{T_{sol-air}}$). The sol-air temperature reflects the superposition effect of ambient temperature and radiation on the exterior envelope surface [53]:

$$T_{sol-air} = T_e + \frac{\alpha I_{rad}}{h_{t,e}} \tag{28}$$

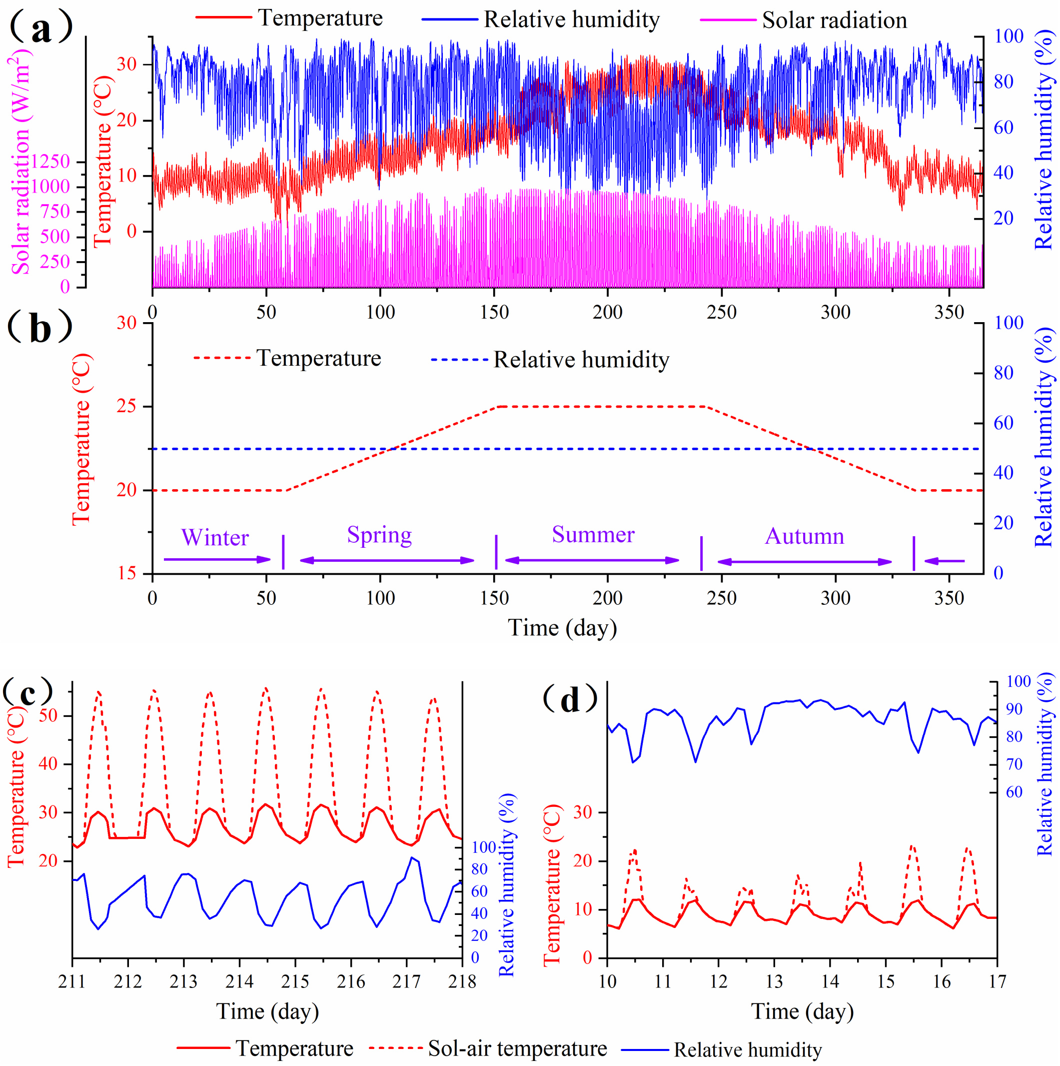

Fig. 3. Climate and interior conditions: (a) annual climate in Rome; (b) annual interior temperature and relative humidity; representative climate during one week in (c) summer and (d) winter

3.2 Numerical solution

The simulations were conducted with the commercial software COMSOL Multiphysics 5.3a, which uses finite element analysis to solve mathematical equations. The General Form PDE interface in COMSOL was used, which allows the user to define and edit the required equations. The general form PDE model in COMSOL is presented as

$$e_a \frac{\partial^2 u}{\partial t^2} + d_a \frac{\partial u}{\partial t} + \nabla \cdot \Gamma = f \tag{29}$$

The terms e_a, d_a, Γ, and f are user-defined coefficients, which are defined by referring to the models in Section 2. The term u is the dependent variable, i.e., relative humidity or temperature.

The meshes of the envelope were generated by COMSOL with an element number of 3972. The finite element equations were solved using the implicit backward differentiation formula solver for time stepping. The relative tolerance was set at 0.001 to guarantee calculation accuracy during the solution process. The calculation was carried out for a three-year period with a time step of 15 min.

3.3 Metric parameters

The metric parameters used in this study comprise three aspects of the interior envelope surface: energy, hygric, and thermal performance.

Energy performance refers to the cumulative heat load ($Q_{gain/loss}$) over a time duration of $\tau_2 - \tau_1$:

$$Q_{gain/loss} = \int_{t=\tau_1}^{t=\tau_2} q_{gain/loss}\, dt \tag{30}$$

The heat gain/loss flux ($q_{gain/loss}$) comprises total, sensible, and latent heat flux:

$$q_{total} = q_{sensible} + q_{latent} \tag{31}$$

$$q_{sensible} = h_{t,i}(T_{x=l} - T_i) \tag{32}$$

$$q_{latent} = L_v h_{m,i}(p_{v,x=l} - p_{v,i}) \tag{33}$$

The hygric and thermal performances comprise moisture loads ($J_{gain/loss}$) over a time duration of $\tau_2 - \tau_1$, partial water vapor pressure amplitude ($p_{v_{amp}}$), and temperature amplitude (T_{amp}):

$$J_{gain/loss} = \int_{t=\tau_1}^{t=\tau_2} j_{gain/loss}\, dt \tag{34}$$

$$p_{v_{amp}} = \left(p_{v_{peak}} - p_{v_{valley}}\right)/2 \tag{35}$$

$$T_{amp} = (T_{peak} - T_{valley})/2 \tag{36}$$

The moisture gain/loss flux ($j_{gain/loss}$) between the envelope and the interior is driven by the concentration difference in partial water vapor pressure, which can be expressed by

$$j = h_{m,i}(p_{v,x=l} - p_{v,i}) \tag{37}$$

Condensation risk assessment was based on ASHRAE Standard 160-2009 [54], which includes the following three criteria:

1. The 30-day running average surface relative humidity is less than 80% when the 30-day running average surface temperature is between 5 and 40 °C;
2. The 7-day running average surface relative humidity is less than 98% when the 7-day running average surface temperature is between 5 and 40 °C;
3. The 24-hour running average surface relative humidity is less than 100% when the 24-hour running average surface temperature is between 5 and 40 °C.

It has been noted that these criteria should be guaranteed at the interior surface and the interfaces between the layers. This logic does not apply to the exterior surface due to its direct exposure to the exterior environment.

Mold growth risk assessment is based on an empirical VTT model developed by Hukka and

Viitanen [55], by which a critical relative humidity (φ_{crit}) can be found, defined as the minimum relative humidity at which mold growth will occur if the material is exposed for a long enough period of time.

$$\varphi_{crit} = \begin{cases} -0.00267 \times T^3 + 0.160 \times T^2 - 3.13 \times T + 100, & T \leq 20 \text{ ℃} \\ 80, & T > 20 \text{ ℃} \end{cases} \tag{38}$$

4. Model validation

4.1 Experimental set-up

Fig. 4 (a) shows the experimental set-up to validate the model. The studied envelopes were placed between a climate chamber and the laboratory environment. The climate chamber provided variable temperature and relative humidity automatically. The laboratory is a small room located in a large building, so there are two building envelopes between the laboratory environment and the exterior environment, ensuring a relatively stable temperature and relative humidity in the laboratory during the experiment. In addition, due to natural convection in the laboratory, the convective heat/mass transfer coefficient between the envelope and the laboratory environment is small, ensuring little heat and moisture transfer between the two. Under these circumstances, the temperature and relative humidity variations within the envelopes were dominated by the climate chamber. Two envelope scenarios were considered, as shown in Fig. 4 (b). The baseline scenario consisted of two HC layers, with an overall dimension of 50 × 50 × 14 cm^3. For the integrated scenario, a PCM layer with a thickness of 2.12 cm was placed between the two HC layers, and the overall dimension was 50 × 50 × 16.12 cm^3. The physical properties of the HC were the same as those shown in Table 1, and the physical properties of the commercial PCM used for the experiment are presented in Table 2 [35].

Fig. 4 (c) and (d) depict the boundary conditions for the two scenarios. In the climate chamber, temperature and relative humidity evolved according to a sinusoidal function with time (day) as the variable: $T = 27.5 + 12.5 \times sin(\pi t/12)$ and $\varphi = 60\% - 35\% \times sin(\pi t/12)$. The temperature and relative humidity in the laboratory environment were relatively stable with fluctuations of less than ± 0.2 °C and ± 1.6%, respectively. For the baseline scenario, the measurement point was at the interface of the two HCs, while for the integrated scenario, the measurement points were the middle of PCM and the second HC.

Several HMP-110 sensors were arranged in the climate chamber, the laboratory environment, and the HC to measure temperature and relative humidity. These sensors have a measurement range of –40 to 80 °C for temperature and 0 to 100% for relative humidity, with accuracies of ±0.2 °C (0–40 °C) and ±1.5% (0–90%), respectively. Thermocouples (type K) were used to measure the temperature in the middle of the PCM; these have a temperature measurement range of –70 to 200°C and an accuracy of ±0.1°C. All sensors were connected to a Keithley 2700 data acquisition system, which has an accuracy of 0.002%. In turn, the Keithley 2700 was connected to a computer to record the experimental data. The experiment was carried out for 48 h with a time step of 120 s for recording the experimental data.

To compare the experimental and simulation results and to ensure validation accuracy, the relative error (θ), root mean square error (RMSE), and coefficient of variation of the root mean square error ($\mathrm{CV}_{(\mathrm{RMSE})}$) were calculated:

$$\theta = \frac{R_e - R_s}{R_e} \times 100\% \tag{39}$$

$$RMSE = \sqrt{\frac{\sum_{i=1}^{n}\left(R_{e_i} - R_{s_i}\right)^2}{n}} \tag{40}$$

$$CV_{(RMSE)} = \frac{RMSE}{\overline{R_e}} \times 100\% \tag{41}$$

where $\mathrm{R_e}$ and $\mathrm{R_s}$ are the experimental and simulation results, respectively; n is the number of data points; $\overline{\mathrm{R_e}}$ is the average value of the experimental result, $\overline{\mathrm{R_e}} = \left(\sum_{\mathrm{i}=1}^{n} R_{e_i}\right)/\mathrm{n}$.

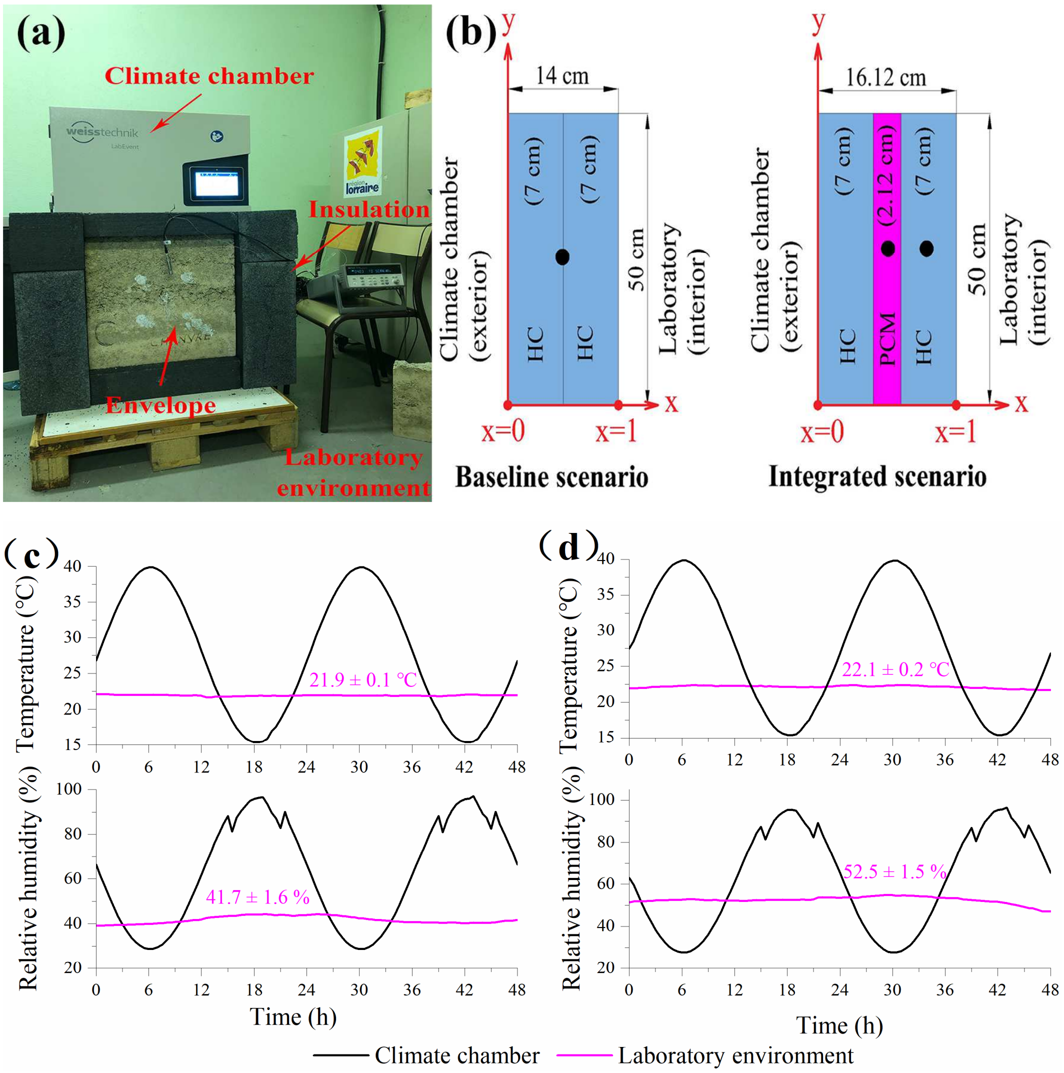

Fig. 4. Experiment for model validation: (a) experimental set-up [21], (b) two envelope scenarios; boundary conditions of (c) baseline scenario and (d) integrated scenario

	PCM
Density (kg/m^3)	810
Thermal conductivity (W/(m·K))	Solid: 0.18; liquid: 0.14
Specific heat capacity (kJ/(kg·K))	Solid: 4.0; liquid: 3.8
Latent heat (kJ/kg)	136.2
Phase transition range (°C)	10–28

Table 2 Physical properties of the PCM for the experiment [35]

4.2 Comparison between experiment and simulation

Fig. 5 (a) and (b) show the simulation and experimental results and their relative errors (right axis). It can be seen that the simulation results are in good agreement with the experimental results in both scenarios. Table 3 summarizes the average, maximum, and minimum relative errors, RMSE, and CV$_{(RMSD)}$. The relative humidity of the baseline scenario reaches the maximum relative error, but this is only 7.5%, while the relative errors for the remaining parameters are less than 3.4%. Moreover, the RMSEs of temperature and relative humidity are less than 0.6 °C and 2.2%, respectively, and all CV$_{(RMSD)}$s are less than 4%. These data suggest that the model exhibits high accuracy in relation to the experiment; thus, it can be considered validated and used to support further simulation studies.

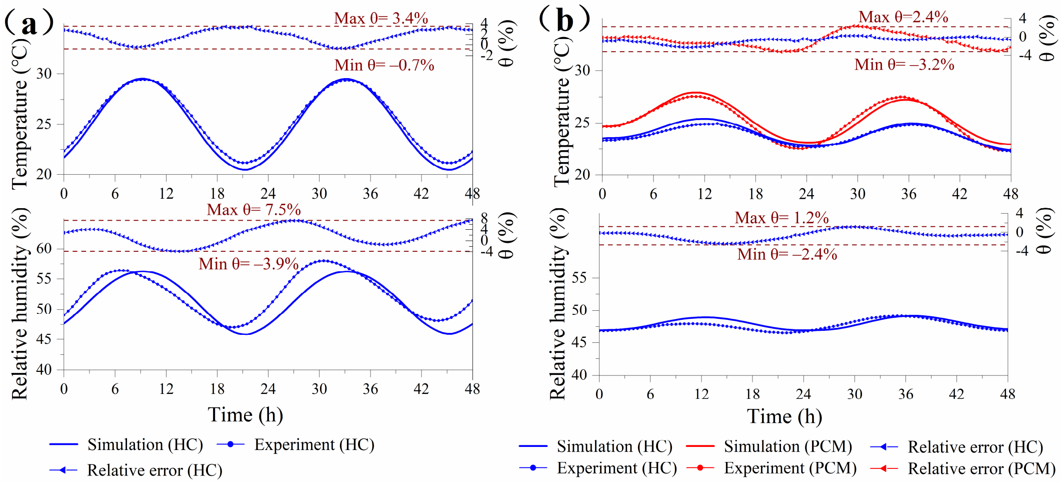

Fig. 5. Comparison between the simulation and experimental results of (a) baseline scenario and (b) integrated scenario

	Baseline scenario		Integrated scenario		
	T_{hc}	φ_{hc}	T_{hc}	φ_{hc}	T_{pcm}
Average θ	1.6%	1.9%	–0.7%	–0.6%	–0.8%
Max θ	3. 4%	7.5%	0.3%	1.2%	2.4%
Min θ	–0.7%	–3.9%	–2.3%	–2.4%	–3.2%
RMSE	0.5 ℃	2.1%	0.2 ℃	0.6%	0.4 ℃
$CV_{(RMSD)}$	1. 9%	3.9%	1.0%	1.2%	1.7%

Table 3 Summary of relative error, RMSE, and $CV_{(RMSD)}$ for baseline and integrated scenarios

5. Results and discussion

In Section 5.1, the impact of moisture transfer on the envelope is analyzed with respect to the baseline scenario. Sections 5.2 and 5.3 consider the impact of the PCM's properties and location in the envelope. In these two sections, the results of the calculations for the third year are used. The heat and moisture loads for seven representative days in summer and winter (see Fig. 3 (c) and (d)) are presented. When the figures express the evolution of the parameters over time (as in Fig. 6 (a), Fig. 7, Fig. 8 (b), etc.), the two-day evolution from a single week is presented for better observation.

In Section 5.4, energy and hygric performance are assessed based on the calculations for the entire third year. Section 5.5 considers the risk of condensation and mold growth based on the three-year simulation calculation.

5.1 Impact of moisture transfer on energy and hygrothermal performance

To study the impact of moisture transfer, the numerical results calculated using the heat and moisture transfer (HMT) model and the heat transfer (HT) model were compared based on the baseline scenario; moreover, the relationships among several main parameters of heat and moisture transfer were analyzed. The HMT model considered the heat and moisture transfer in the HC and heat transfer in the PCM. The HT model considered only heat transfer in the HC and the PCM, and the thermophysical parameters of the HC were the constant terms shown in Table 1.

Fig. 6 (a) presents the heat fluxes of the HMT and HT models in summer and winter, and their corresponding loads are plotted in Fig. 6 (b). By focusing on sensible heat in the HMT model and total heat in the HT model, it can be seen that their variations and values are similar. The slight difference between these is caused by the thermophysical parameters of HC: The thermal conductivity and heat capacity of HC are higher in the HMT model due to the consideration of moisture. In addition, these values are both lower than the total heat flux in the HMT model. The latent heat flux in the HMT model is small and fluctuates around the x-axis (0 W/m^2). As for the heat loads, the total heat load in the HT model is less than that in the HMT model for both seasons, indicating that the total heat load was underestimated without considering moisture transfer. Further, since the sensible heat in the HMT model is close to the total heat in the HT model, and the total heat is the superposition of the sensible and latent heats in the HMT model, it can be inferred that the latent heat load is the main reason for the total heat load difference between the two models. Based on the calculations, the latent heats are 10.4% and 3.1% of the total heat load in summer and winter, respectively, showing that the impact of latent heat on the total heat is greater in summer.

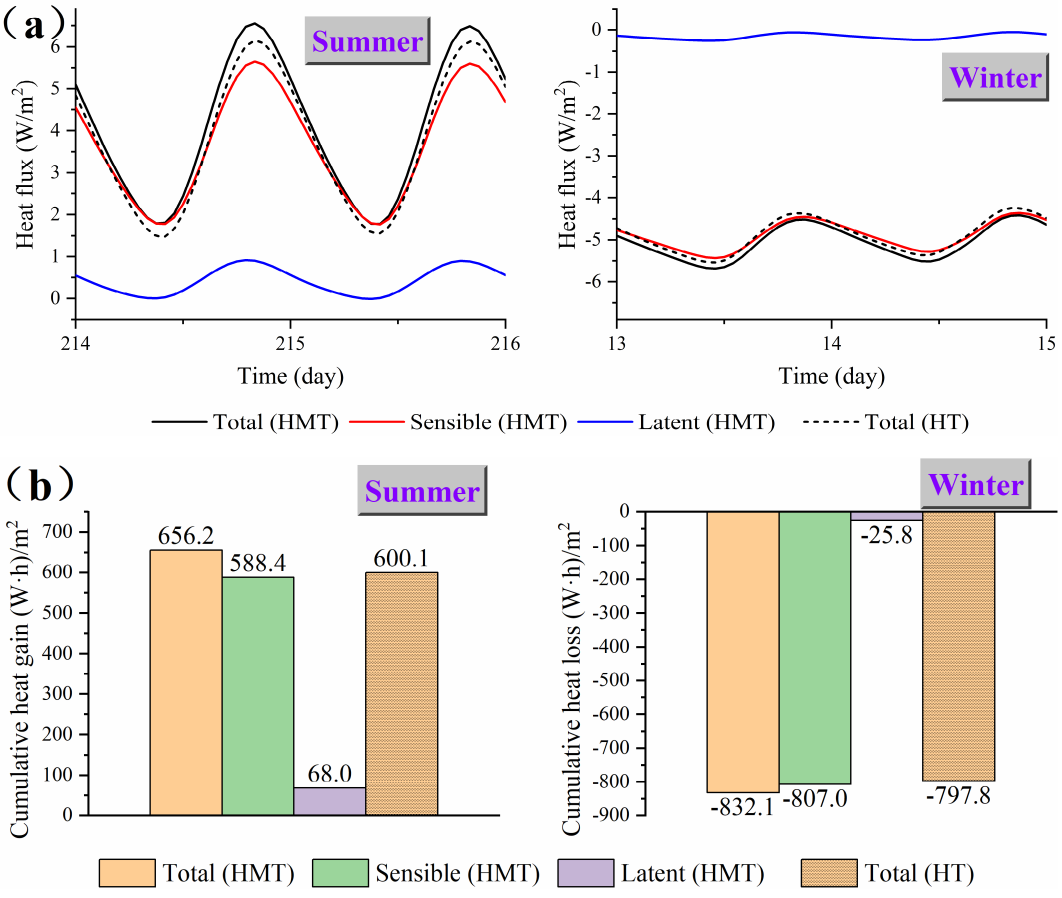

Fig. 6. Comparison between HMT and HT models: (a) heat fluxes; (b) heat loads

Fig. 7 illustrates the transformation between moisture transfer and latent heat transfer by analyzing the relationship between partial water vapor pressure, moisture flux, and latent heat flux. The driving force for moisture transfer between the envelope surface and the interior is the concentration difference in partial water vapor pressure, and the partial water vapor pressure on the interior surface is jointly affected by temperature and relative humidity, with temperature playing the dominant role. On the one hand, the partial water vapor pressure variation is highly consistent with temperature variation, indicating the dominant role of temperature. On the other hand, a slight time delay (1.6 and 1.7 h in summer and winter, respectively) is observed between changes in partial water vapor pressure and changes in temperature, suggesting a weak effect of relative humidity on partial water vapor pressure.

Concerning partial water vapor pressure, moisture flux, and latent heat flux, they show similar variation trends. The conversion factors between the partial water vapor pressure gradient and moisture flux and between the moisture flux gradient and latent heat flux are water vapor permeability (a function of relative humidity) and latent heat of evaporation (a function of temperature), respectively. In summer, the water vapor permeability fluctuates from 3.8×10^{-11} to 3.9×10^{-11} $\mathrm{kg/(Pa{\cdot}m{\cdot}s)}$ and the latent heat of evaporation fluctuates from 2.438×10^{6} to 2.440×10^{6} $\mathrm{J/kg}$, while in winter, they fluctuate even less. Since the orders of magnitude of water vapor permeability and latent heat of evaporation are lower than those of the partial water vapor pressure gradient and the moisture flux gradient, respectively, they can be regarded as constant, which explains the similar variation trends between partial water vapor pressure, moisture flux, and latent heat flux. Thus, the moisture flux/load is highly correlated with the latent heat flux/load, and both are mainly dominated by temperature.

To sum up, moisture transfer is crucial since it correlates with the indoor moisture environment and significantly affects the latent/total heat and, thus, the energy performance.

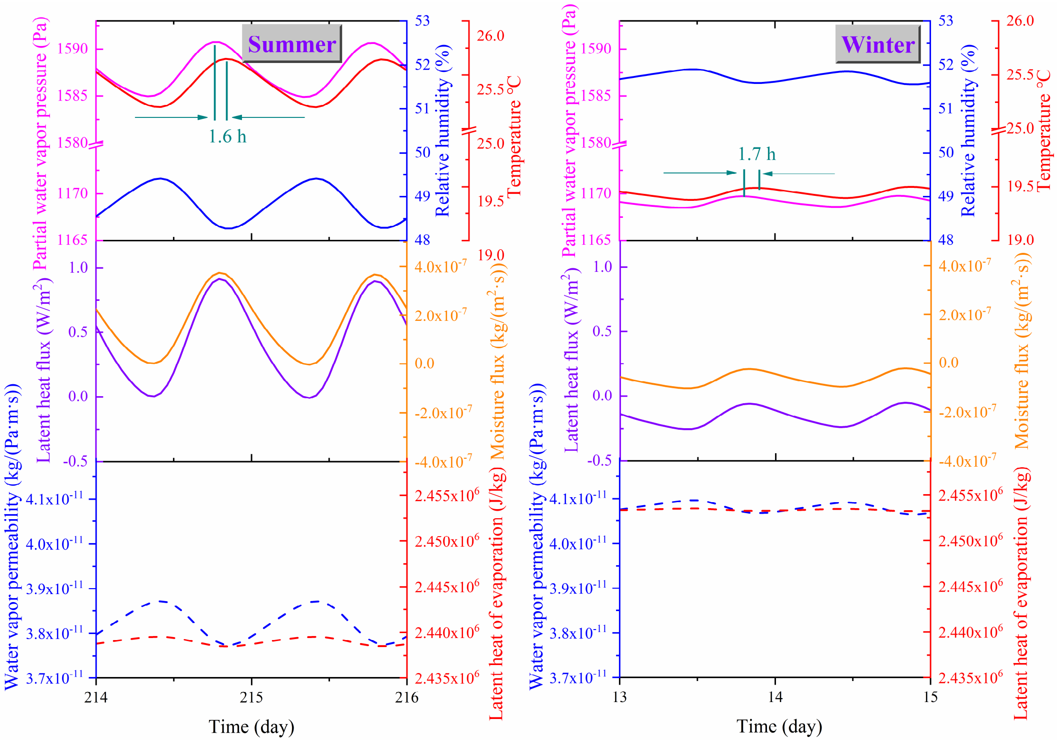

Fig. 7. Relationship between temperature, relative humidity, partial water vapor pressure, moisture flux, and latent heat flux

5.2 Impact of PCM and its location on energy and hygrothermal performance

Fig. 8 (a) shows the cumulative heat load and moisture load in summer and winter for the five scenarios. For the integrated scenarios, the total heat gain decreases with the movement of the PCM toward the interior, and its values are mostly lower than that of the baseline scenario. Fig. 8 (c) summarizes the heat load reductions of the integrated scenarios compared to the baseline scenario. In summer, the total heat gain is reduced for all integrated scenarios except scenario 1/5, since the PCM placed on the outermost layer absorbs/releases more energy than does the HC. The heat load reductions for scenarios 2/5, 3/5, and 4/5 are 3.6%, 6.6%, and 8.2%, respectively. In winter, the heat load is less affected by the PCM, with a reduction of less than 1.5%. Notably, as illustrated in Fig. 8 (a), scenario 4/5 has the largest sensible heat load but the smallest total heat load in both seasons. Moreover, the latent heat difference among the scenarios is higher than the sensible heat difference: The maximum difference among the latent heat loads is about 3.6 and 1.3 times that for sensible heat loads in summer and winter, respectively. This indicates that the latent heat loads play a crucial role in determining the magnitude of the total heat loads in different scenarios; as the PCM moves toward the interior, the latent heat and its percentage (ratio of latent heat load to total heat load; right axis) decrease. The latent heat percentages for scenario 4/5 (2.3% in summer and 0.4% in winter) are much smaller than those for scenario 1/5 (13.5% in summer and 3.3% in winter).

The moisture loads are highly consistent with the latent heat loads. For the integrated scenarios, the closer the PCM is to the interior, the lower the moisture gain in summer and the lower the moisture loss in winter. Further, the difference between the moisture gain and moisture loss decreases as the PCM moves closer to the interior, which is favorable in terms of the moisture equilibrium within the HC.

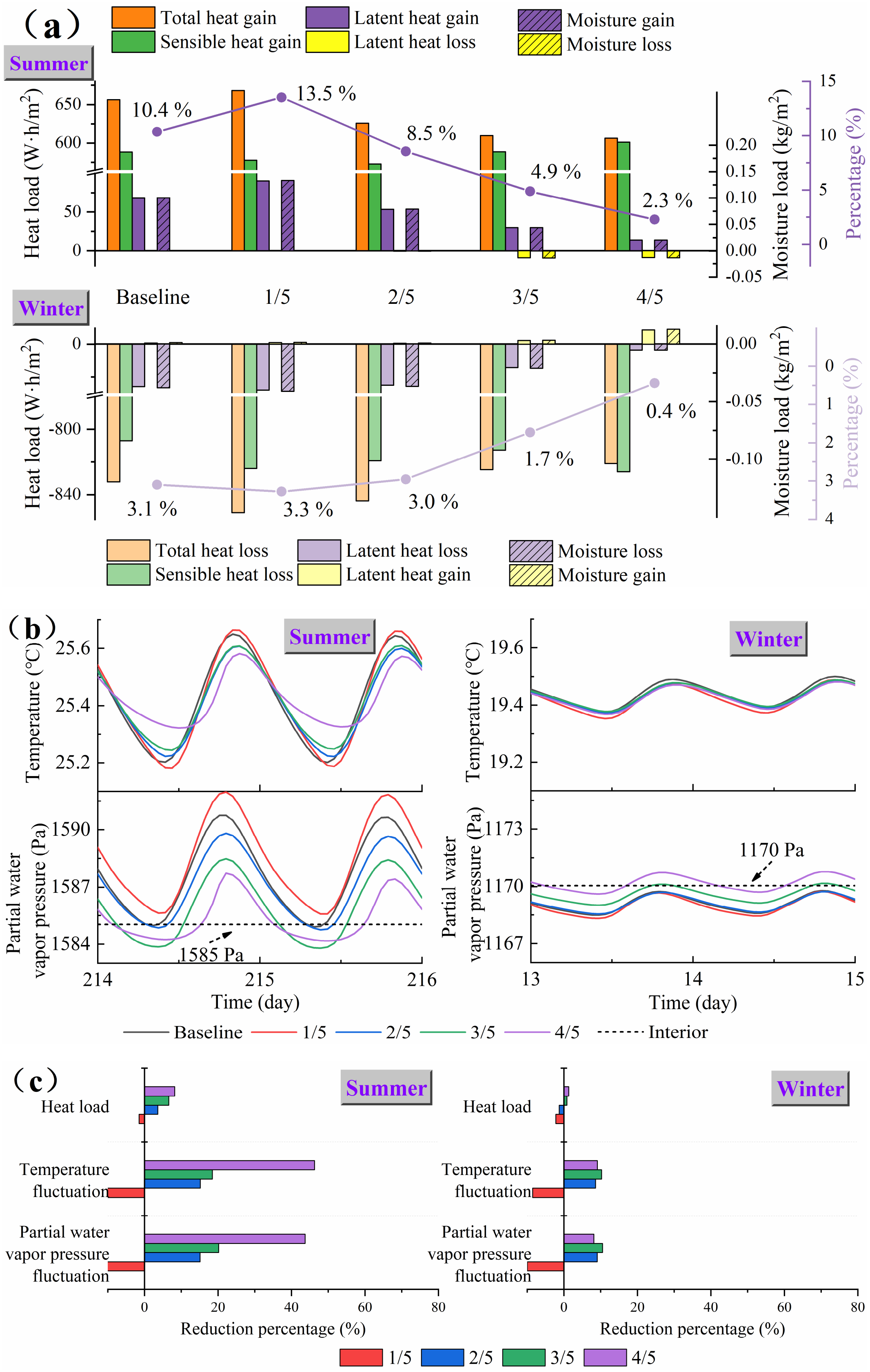

Fig. 8. Impact of PCM presence and location: (a) cumulative heat load and moisture load; (b) variation of

temperature and partial water vapor pressure; (c) reduction of heat load, temperature fluctuation, and partial water vapor pressure fluctuation compared to baseline scenario

Fig. 8 (b) shows the variations of temperature and partial water vapor pressure and explains the different moisture and latent heat loads among the scenarios. First, the temperature and partial water vapor pressure amplitudes decrease with the presence of the PCM, except in scenario 1/5; these also decrease as the PCM moves closer to the interior, especially in summer. Fig. 8 (c) shows the temperature and partial water vapor pressure amplitude reductions compared to the baseline scenario. In summer, the temperature fluctuations in scenarios 2/5, 3/5, and 4/5 are reduced by 15.2%, 18.5%, and 46.3%, respectively, and the partial water vapor pressure fluctuations are reduced by 15.1%, 20.2%, and 43.7%, respectively. In winter, the corresponding reductions in scenarios 2/5, 3/5, and 4/5 are small and similar, with a mean reduction of 9.3%. Hence, scenarios 2/5, 3/5, and 4/5 can reduce indoor temperature and relative humidity fluctuations to improve thermal and hygric comfort, especially in summer.

Furthermore, the partial water vapor pressure moves gradually toward the reference line (interior) from scenario 1/5 to scenario 4/5, meaning that their values gradually decrease in summer and increase in winter. In particular, the curves for scenarios 3/5 and 4/5 move to such a situation that they fluctuate repeatedly around the reference line, especially for scenario 4/5. As explained previously, the moisture flux and latent heat flux between the envelope and the interior environment are affected by partial water vapor pressure. Therefore, with the movement of the PCM closer to the interior, the moisture and latent heat loads’ gains in summer and losses in winter gradually decrease.

In sum, among the scenarios, scenario 4/5 shows the greatest advantage in terms of improving indoor hygrothermal comfort and saving energy.

5.3 Impact of PCM properties on energy and hygrothermal performance

In this section, the impact of PCM thickness, latent heat, and phase transition range on energy and hygrothermal performance is investigated based on scenario 4/5. The physical properties of the base PCM are a thickness of 0.01m, a latent heat of 90.4 kJ/(kg·K), and a phase transition range of 24–28 °C. When the impact of one of these parameters is studied, the remaining two parameters remain unchanged. The main metric parameters concerned are the total heat load, temperature, and partial water vapor pressure fluctuations, as well as their reductions compared to the baseline scenario.

5.3.1 Impact of PCM thickness

Fig. 9 (a) shows the heat and moisture loads for different PCM thicknesses (0.01, 0.02, and 0.03 m). Fig. 9 (b) shows the variations of temperature and partial water vapor pressure. With the increase in PCM thickness, the total heat/moisture load, temperature fluctuation, and partial water vapor pressure fluctuations all decrease, especially in summer. This is because the increase in PCM thickness enhances the heat storage capacity and thermal resistance of the envelope, and the thermal storage capacity enhancement is greater in summer.

Fig. 9 (c) shows the percentage reduction in heat load and partial water vapor pressure/temperature fluctuations for PCM thicknesses of 0.01, 0.02, and 0.03 m, compared to the baseline scenario. It can be observed that a thicker PCM is more conducive to improving energy and hygrothermal performance, especially in summer. In summer, the heat loads of 0.01, 0.02, and 0.03 m are reduced by 7.8%, 10.5%, and 13.9%, respectively, and the partial water vapor pressure/temperature fluctuations are reduced by more than 43.6%, 64.2%, and 76.5%, respectively. In winter, the reductions are 1.2%, 2.4%, and 5.0% for heat load and approximately 8.6%, 25.8%, and 38.8% for the partial water vapor pressure/temperature fluctuations. Although the reductions are smaller in winter than in summer, they still contribute to energy savings and the stability of indoor temperature and relative humidity. Hence, the energy and hygrothermal performance of the integrated envelope can be optimized by increasing PCM thickness, especially in summer.

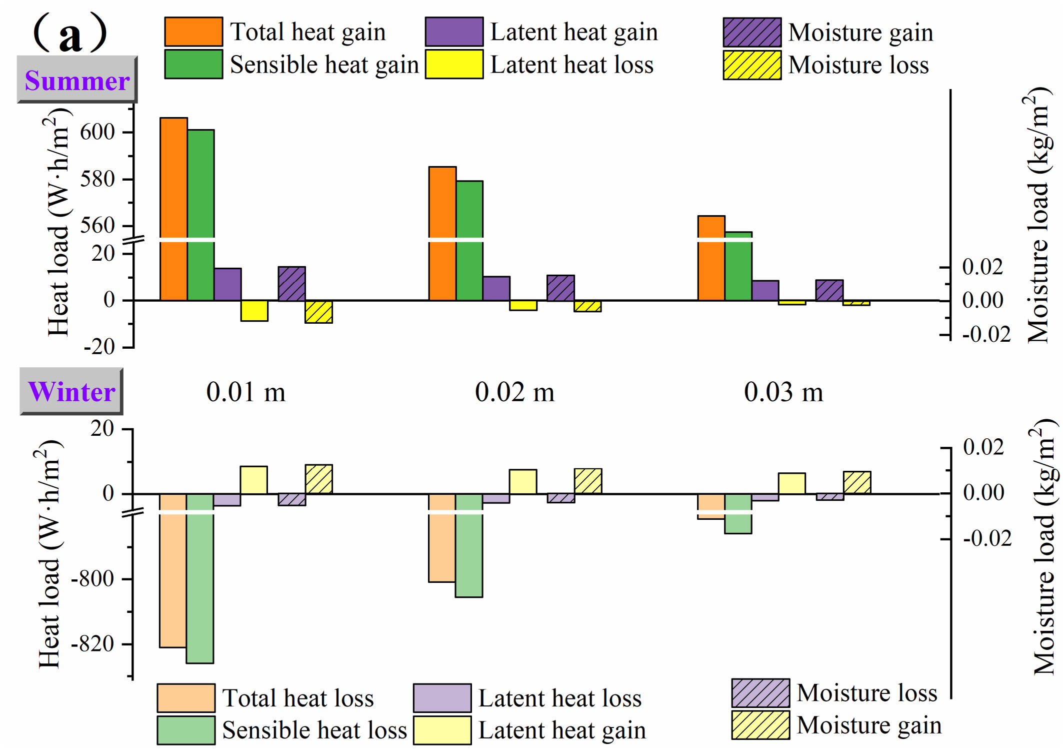

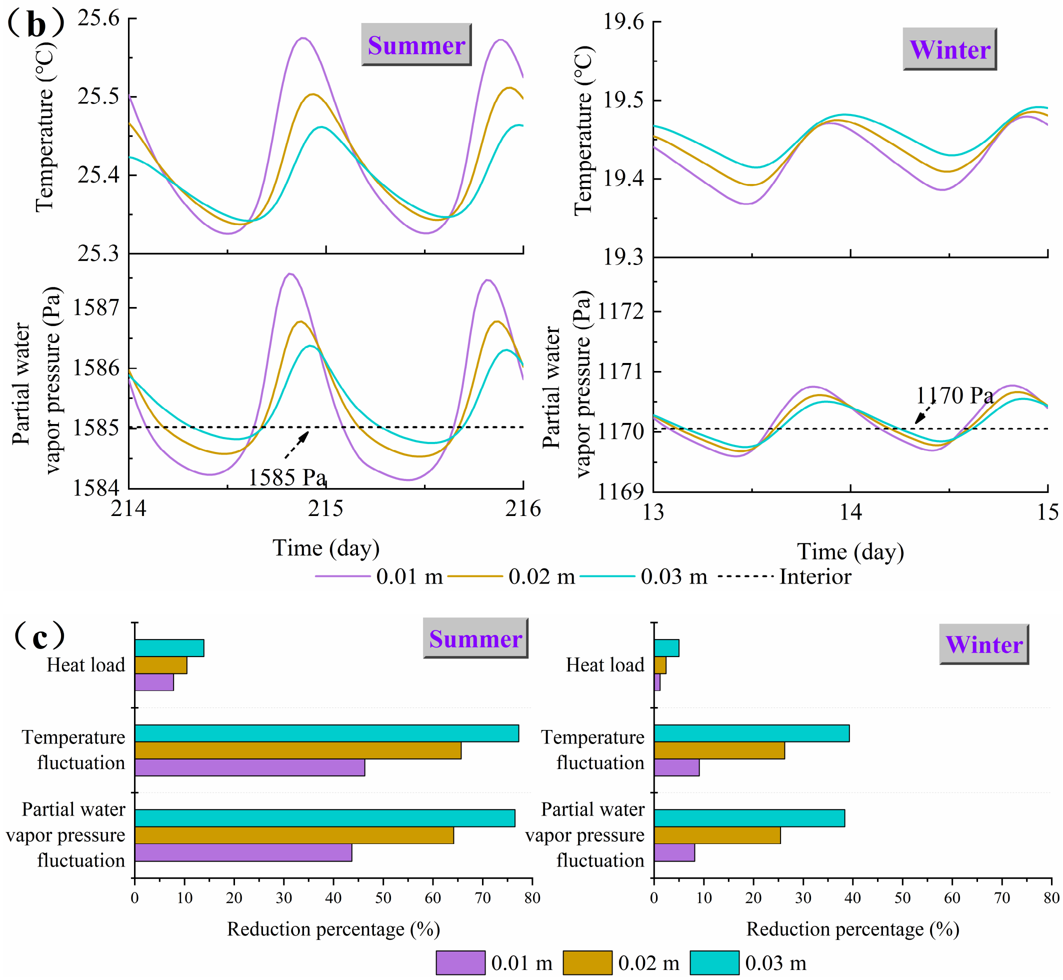

Fig. 9. Impact of PCM thickness: (a) cumulative heat load and moisture load; (b) variation of temperature and partial water vapor pressure; (c) reduction of heat load, temperature fluctuation, and partial water vapor pressure fluctuation compared to baseline scenario

5.3.2 Impact of PCM latent heat

The impact of PCM latent heat (62.9, 90.4, 117.8, and 145.3 kJ/kg) on heat and moisture load is shown in Fig. 10 (a). In summer, both the heat and moisture loads decrease with the increase in latent heat. As presented in Fig. 10 (c), the heat load reductions for 62.9, 90.4, 117.8, and 145.3 kJ/kg are 7.1%, 7.5%, 7.7%, and 8.0%, respectively, compared to the baseline. However, in winter, the heat loads are less affected by the PCM latent heat load, with almost identical reductions of less than 1.5%. This is because the PCM with a phase transition range of 24–28 °C is in a solid state and thus not activated in winter.

Fig. 10 (b) presents the variations of temperature and partial water vapor pressure. In summer, a clear difference can be observed: The temperature and partial water vapor pressure amplitudes decrease with the increase in PCM latent heat. Compared to the baseline scenario, the temperature amplitudes of 62.9, 90.4, 117.8, and 145.3 kJ/kg are reduced by 40.3%, 46.3%, 51.2%, and 57.2%, respectively, and the partial water vapor pressure amplitudes are reduced by 38.3%, 43.7%, 48.4%, and 55.2%, respectively (see Fig. 10 (c)). However, in winter, the temperature and partial water vapor pressure curves for the different PCM latent heats almost overlap and the reductions are similar, reflecting the negligible effect of latent heat on hygrothermal performance. Hence, increasing PCM latent heat to optimize envelope performance is more likely to be suggested in summer.

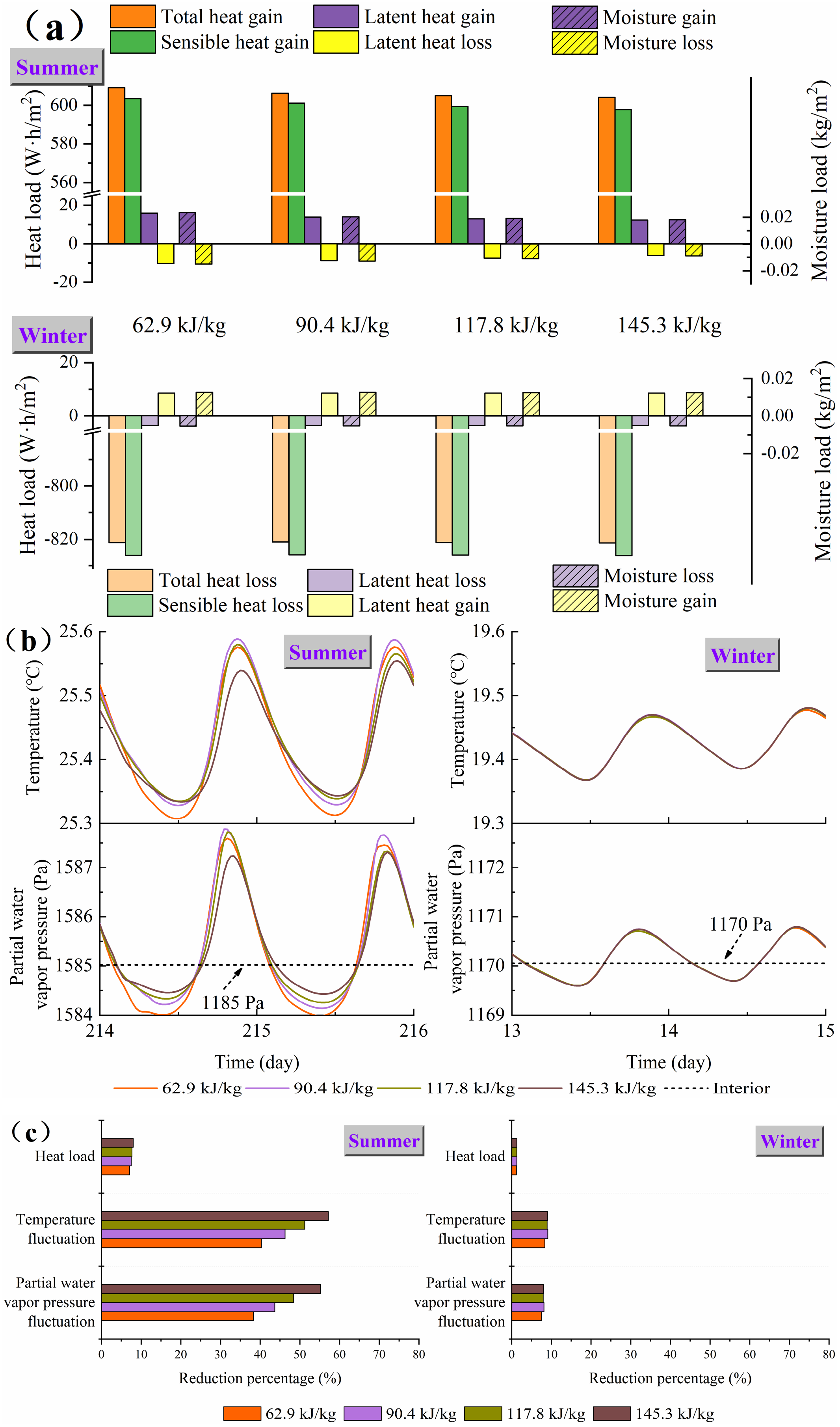
（a）
Total heat gain
Sensible heat gain
Latent heat gain
Latent heat loss
Moisture gain
Moisture loss
Summer
Heat load (W·h/m^2)
600
580
560
20
0
-20
Moisture load (kg/m^2)
0.02
0.00
-0.02
62.9 kJ/kg
90.4 kJ/kg
117.8 kJ/kg
145.3 kJ/kg
Winter
Heat load (W·h/m^2)
20
0
-800
-820
Moisture load (kg/m^2)
0.02
0.00
-0.02
Total heat loss
Sensible heat loss
Latent heat loss
Latent heat gain
Moisture loss
Moisture gain
（b）
Summer
Temperature (°C)
25.6
25.5
25.4
25.3
Partial water vapor pressure (Pa)
1587
1586
1585
1584
1185 Pa
214
215
216
Time (day)
Winter
Temperature (°C)
19.6
19.5
19.4
19.3
Partial water vapor pressure (Pa)
1172
1171
1170
1169
1170 Pa
13
14
15
Time (day)
62.9 kJ/kg
90.4 kJ/kg
117.8 kJ/kg
145.3 kJ/kg
Interior
（c）
Summer
Heat load
Temperature fluctuation
Partial water vapor pressure fluctuation
0
10
20
30
40
50
60
70
80
Reduction percentage (%)
Winter
Heat load
Temperature fluctuation
Partial water vapor pressure fluctuation
0
10
20
30
40
50
60
70
80
Reduction percentage (%)
62.9 kJ/kg
90.4 kJ/kg
117.8 kJ/kg
145.3 kJ/kg

Fig. 10. Impact of PCM latent heat: (a) cumulative heat load and moisture load; (b) variation of temperature and partial water vapor pressure; (c) reduction of heat load, temperature fluctuation, and partial water vapor pressure fluctuation compared to baseline scenario

5.3.3 Impact of PCM phase transition range

In this subsection, the impact of the PCM phase transition range is studied; the different ranges are 16–20, 20–24, 24–28, and 28–32 °C. Fig. 11 shows the middle temperature of PCM for these phase transition ranges. The PCM temperatures for the phase transition ranges of 24–28 °C in summer and 16–20 °C in winter differ significantly from the temperatures for the remaining phase transition ranges, which are characterized by fewer temperature fluctuations since their PCMs are undergoing a phase change process. In contrast, the PCMs in the remaining phase transition ranges are mostly in the solid or liquid state, which does not take full advantage of the PCM.

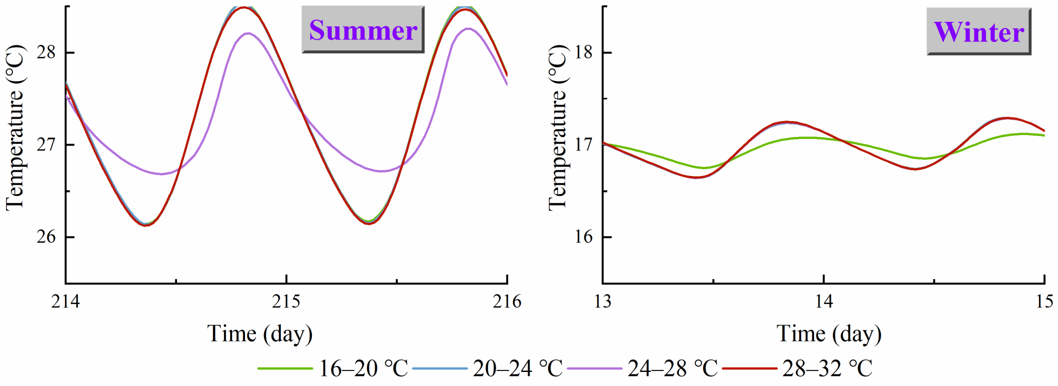

Fig. 11. Middle temperature of PCMs for different PCM phase transition ranges

Fig. 12 (a) depicts the heat and moisture loads. In summer, the smallest total heat gain occurs in the 24–28 °C phase transition range. Inversely, the largest heat loss corresponds to the 16–20 °C phase transition range in winter, as the innermost PCM layer easily absorbs energy from the high temperature side (interior). Fig. 12 (c) summarizes the total heat load reduction compared to the baseline scenario. The reductions for 16–20, 20–24, 24–28, and 28–32 °C are 7.5%, 7.6%, 7.7%, and 7.1%, respectively, in summer and 0.6%, 1.3%, 1.3%, and 1.3%, respectively, in winter. Thus, the 24–28 °C phase transition range in summer contributes to energy savings. As for the improvement of hygrothermal performance, the phase transition ranges of 24–28 °C in summer and 16–20 °C in winter both make contributions. In Fig. 12 (b), the corresponding temperature and partial water vapor pressure fluctuations are reduced in both seasons. Compared to the baseline scenario, the temperature and partial water vapor pressure amplitude reductions are 46.2% and 43.7% for the 24–28 °C phase transition range in summer, almost three times the reductions for the remaining phase transition ranges. Similarly, the temperature and partial water vapor pressure amplitude reductions are as high as 55.8% and 55.9% for the 16–20 °C phase transition range in winter (see Fig. 12 (c)). Therefore, when the phase transition range ensures that the PCM undergoes a phase change, indoor hygrothermal comfort can be improved in both seasons and energy savings can be achieved in summer.

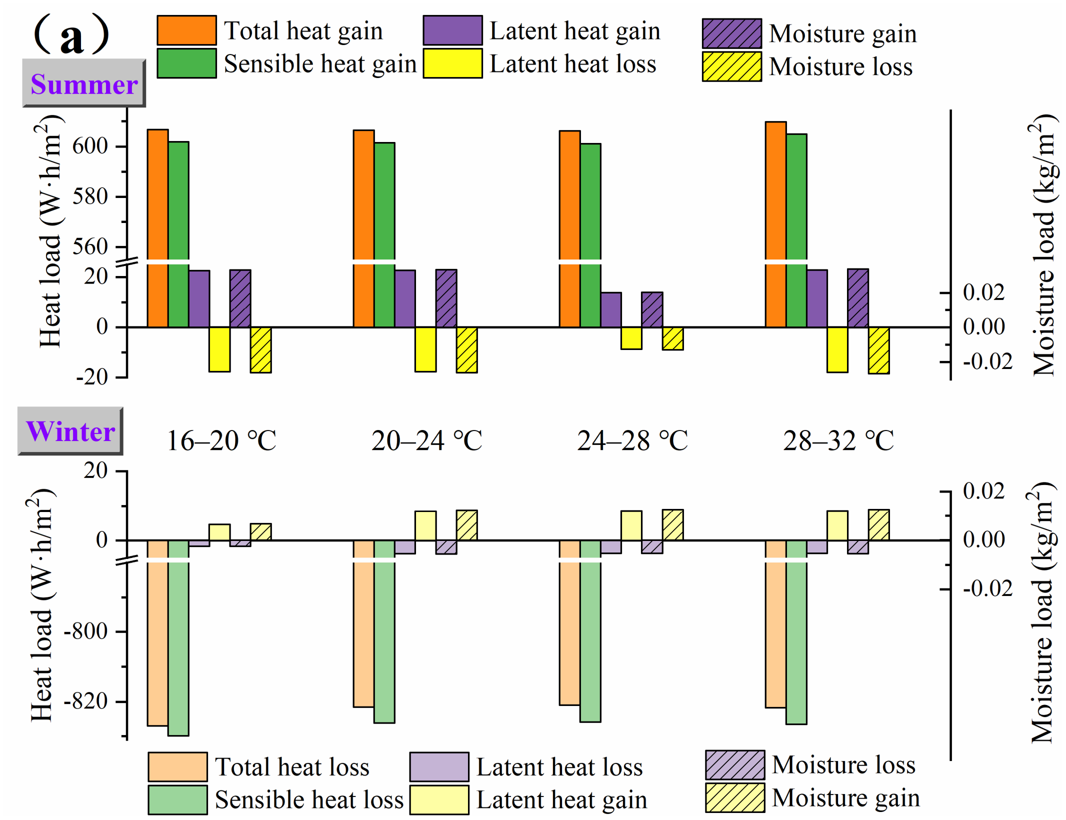
(a)
Total heat gain
Sensible heat gain
Latent heat gain
Latent heat loss
Moisture gain
Moisture loss
Summer
Heat load (W·h/m^2)
600
580
560
20
0
-20
Moisture load (kg/m^2)
0.02
0.00
-0.02
Winter
16–20 °C
20–24 °C
24–28 °C
28–32 °C
20
0
-800
-820
Heat load (W·h/m^2)
0.02
0.00
-0.02
Moisture load (kg/m^2)
Total heat loss
Sensible heat loss
Latent heat loss
Latent heat gain
Moisture loss
Moisture gain

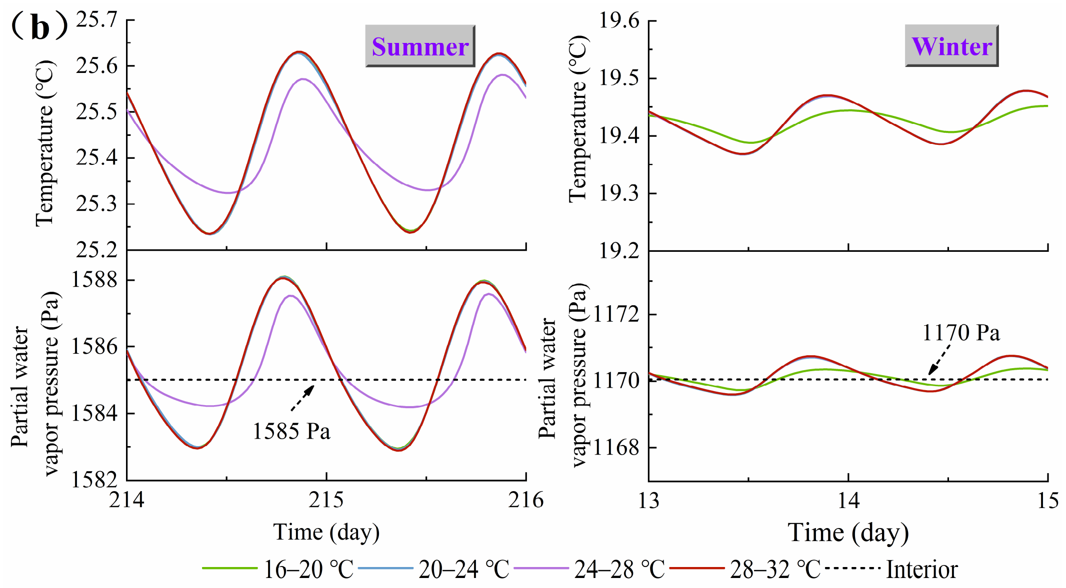
(b)
Summer
Temperature (°C)
25.7
25.6
25.5
25.4
25.3
25.2
Partial water vapor pressure (Pa)
1588
1586
1584
1582
1585 Pa
214
215
216
Time (day)
Winter
Temperature (°C)
19.6
19.5
19.4
19.3
19.2
Partial water vapor pressure (Pa)
1172
1170
1168
1170 Pa
13
14
15
Time (day)
16–20 °C
20–24 °C
24–28 °C
28–32 °C
Interior

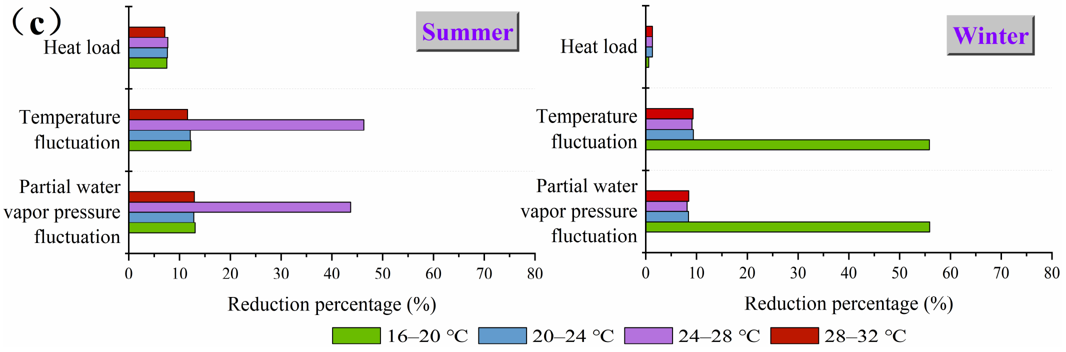
(c)
Summer
Heat load
Temperature fluctuation
Partial water vapor pressure fluctuation
0
10
20
30
40
50
60
70
80
Reduction percentage (%)
Winter
Heat load
Temperature fluctuation
Partial water vapor pressure fluctuation
0
10
20
30
40
50
60
70
80
Reduction percentage (%)
16–20 °C
20–24 °C
24–28 °C
28–32 °C

Fig. 12. Impact of PCM phase transition range: (a) cumulative heat load and moisture load; (b) variation of temperature and partial water vapor pressure; (c) reduction of heat load, temperature fluctuation, and partial water vapor pressure fluctuation compared to baseline scenario

Several prior studies have reported similar results in terms of PCM location [10, 56, 57], thickness [11], latent heat [12, 13], and phase transition range [58, 59]. However, these studies focused only on the heat transfer and thermal performance (sensible heat load) of the envelope. In this study, due to the presence of hygroscopic HC, the latent heat load caused by moisture transfer increases the complexity of the total heat load. This phenomenon is more pronounced when studying the impact of PCM location. If only the sensible heat load is considered, the scenarios with the smallest heat gain in summer and the smallest heat loss in winter are 2/5 and 3/5, respectively, either of which would undoubtedly be the wrong choice. When considering the effect of latent heat load, the optimal PCM location moves to the interior in both seasons because of the decreasing latent heat percentage. The effect of latent heat load discussed in Section 5.3 is smaller because the study is based on scenario 4/5, in which the latent heat load accounts for only 2.3% and 0.4% of the total heat load in summer and winter, respectively. If the studies are conducted based on scenarios with the PCM away from the interior, it can be inferred that the latent heat load still plays an important role in the energy performance results. Therefore, when evaluating the energy performance of an envelope that can transfer moisture with the interior environment, the superposition effect of the sensible and latent heat loads, rather than just sensible heat loads, needs to be considered.

5.4 Assessment of energy and hygric performance

Fig. 13 shows the annual heat loads of the HMT and HT models. For the HMT model, the heat loads for the integrated scenarios decrease as the PCM moves closer to the interior. Most of these are lower than the heat loads for the baseline, and the reduction of heat gain is more obvious than the reduction of heat loss. Scenario 4/5 has the smallest heat gain and loss, and the reduction of heat gain is 13.3% compared to the baseline, which is much higher than the heat loss reduction of only 0.5%. Hence, PCMs are more capable of reducing heat gain, and the closer the PCM to the interior, the more the heat gain reduction.

Concerning the difference between the HMT and HT models, the heat gains and losses are always higher in the HMT model than in the HT model due to moisture transfer. Thus, failing to consider moisture transfer leads to an underestimation of the annual heat load, which is reflected by the heat load reduction percentage in the HT model (right axis) compared to the HMT model. The heat gain underestimation for the baseline scenario is as high as 12.1%. For the integrated scenarios, the underestimation decreases as the PCM moves toward the interior, with the lowest underestimation being 2.6% for scenario 4/5. For heat loss, the underestimations are all below 5%.

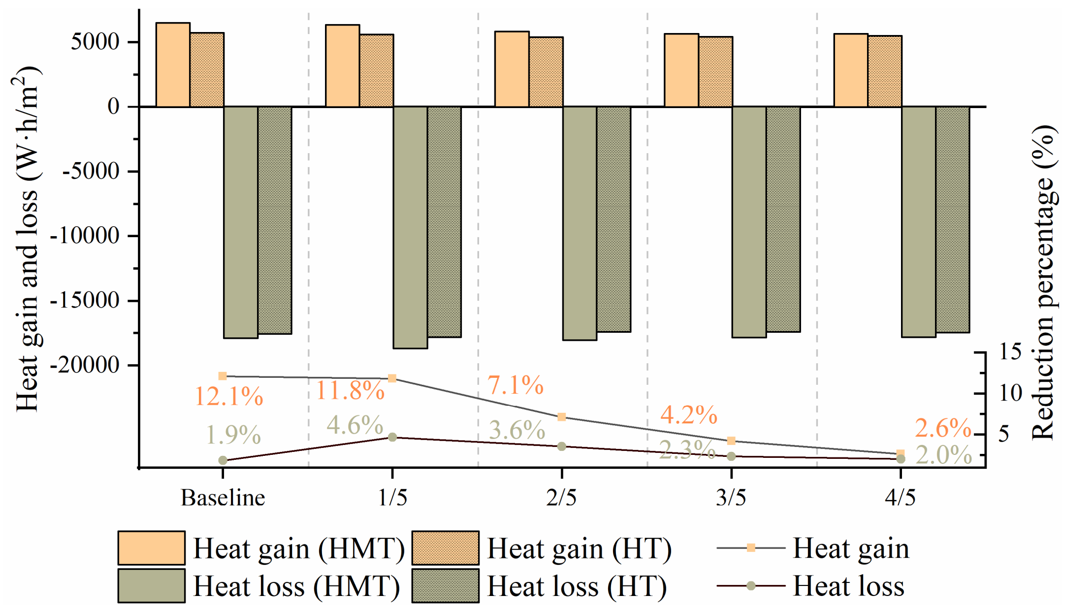

Fig. 13. Annual heat gain and loss for HMT and HT models

Fig. 14 (a) and (b) present the annual heat and moisture loads expressed in a seasonal format. For the heat load, scenario 4/5 is noteworthy in almost every season. In summer, this scenario has the smallest heat gain and the largest energy savings (11.5%) compared to the baseline scenario. Similarly, it also reduces heat loss in winter, but the reduction is less pronounced than in summer, with less than a 1% energy savings compared to the baseline scenario. In spring and autumn when heat loss is predominant, scenario 4/5 also slightly reduces heat loss.

Moisture performance is assessed from two aspects. First, the climate relative humidity is moderate in summer (average relative humidity of 63.9%) and high in spring, autumn, and winter (average relative humidities of 77.9%, 78.9%, and 81.5%, respectively). Hence, an ideal situation for the interior would involve less moisture gain in summer and more moisture loss in spring, autumn, and winter. From this point of view, scenario 4/5 is the optimum scenario. Second, the moisture content within the HC in contact with the interior needs to be well equilibrated, which requires a slight difference between moisture gain and loss. The baseline scenario and scenarios 1/5 and 2/5 have almost no moisture loss in summer and almost no moisture gain in winter. Similarly, scenarios 2/5 and 3/5 have almost no moisture gain in autumn. In contrast, scenario 4/5 better meets this requirement in all seasons as it has both moisture gain and loss, and the difference between moisture gain and loss is smaller than in the other scenarios.

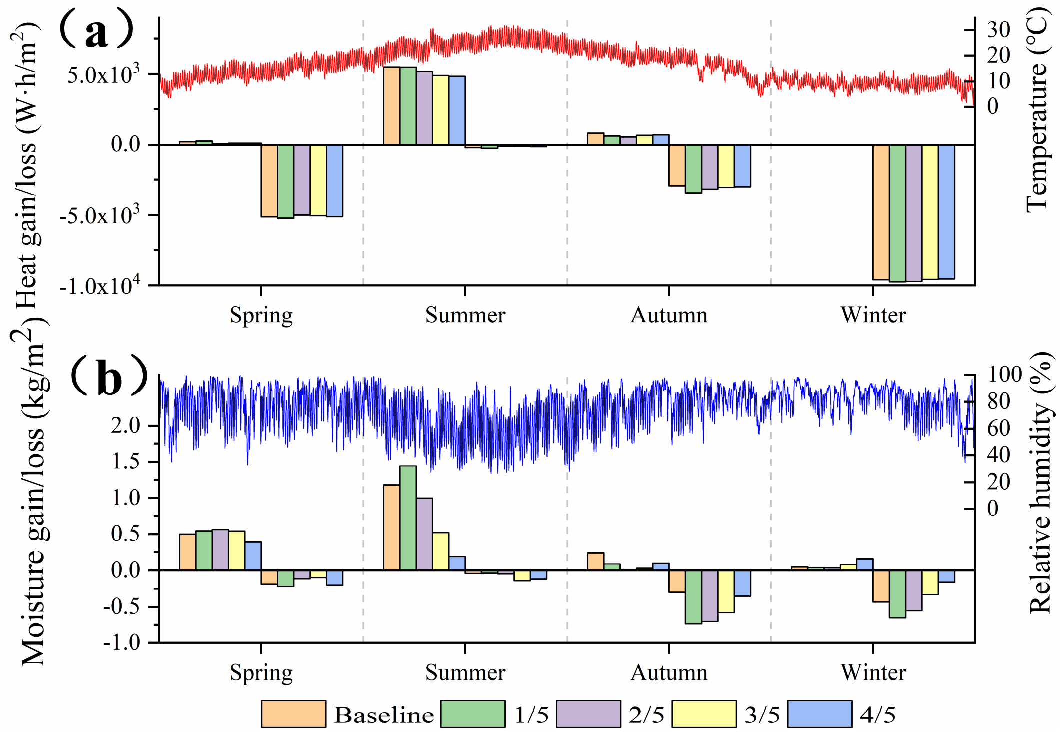

Fig. 14. Annual comparison for different scenarios of (a) heat load and (b) moisture load

5.5 Assessment of condensation and mold growth risk

PCM is a moisture impermeable material and seems to cause high relative humidity in localized locations of the integrated scenarios. This section covers the three-year simulation conducted to assess the relative humidity and temperature behaviors at different locations for the different scenarios to assess the risk of condensation and mold growth.

Fig. 15 (a) shows the relative humidity variation during the three years. Generally, the relative humidity at each location under different scenarios shows periodic variation with a one-year cycle, fixing the relative humidity within a certain range year after year. Taking location P_1 in scenario 4/5 as an example, its relative humidity increases starting in autumn and reaches its highest values in winter, and then it decreases in spring and drops to its lowest values in summer, with an overall relative humidity range of 44.0% to 60.9%. Concerning the locations of each scenario, location H_1 (interior surface) in each scenario has the most stable relative humidity throughout the year. Conversely, the locations close to the exterior (such as location H_4 in the baseline scenario, location P_1 in scenario 1/5, etc.) are more likely to experience a large relative humidity fluctuation both yearly and daily. Because the relative humidity variation within the HC is highly affected by temperature, an increase/decrease in temperature leads to the evaporation/condensation of moisture within the HC, which increases/decreases the relative humidity. Thus, the locations with high temperature fluctuations always have high relative humidity fluctuations, both daily and annually. For these scenarios, the maximal relative humidity is always below 75% at each location. Therefore, criteria a, b, and c in ASHRAE Standard 160-2009 are confirmed.

Fig. 15 (b) presents the point group of temperature and relative humidity on a three-year scale to assess the risk of mold growth. A visually expansive range of temperatures and relative humidities can also be observed at locations close to the exterior of each scenario, especially scenario 1/5. Location P_2 in scenario 2/5 has the highest mold growth risk with a relative humidity slightly below the φ_{crit}. Scenario 4/5 remains particularly far from the φ_{crit} with the smallest temperature and relative humidity variations, indicating the smallest risk of mold growth. Thus, the integrated scenarios ensure that the relative humidity is always below φ_{crit}.

Consequently, considering the periodic variations, a low risk of condensation and mold growth can be guaranteed for a long time.

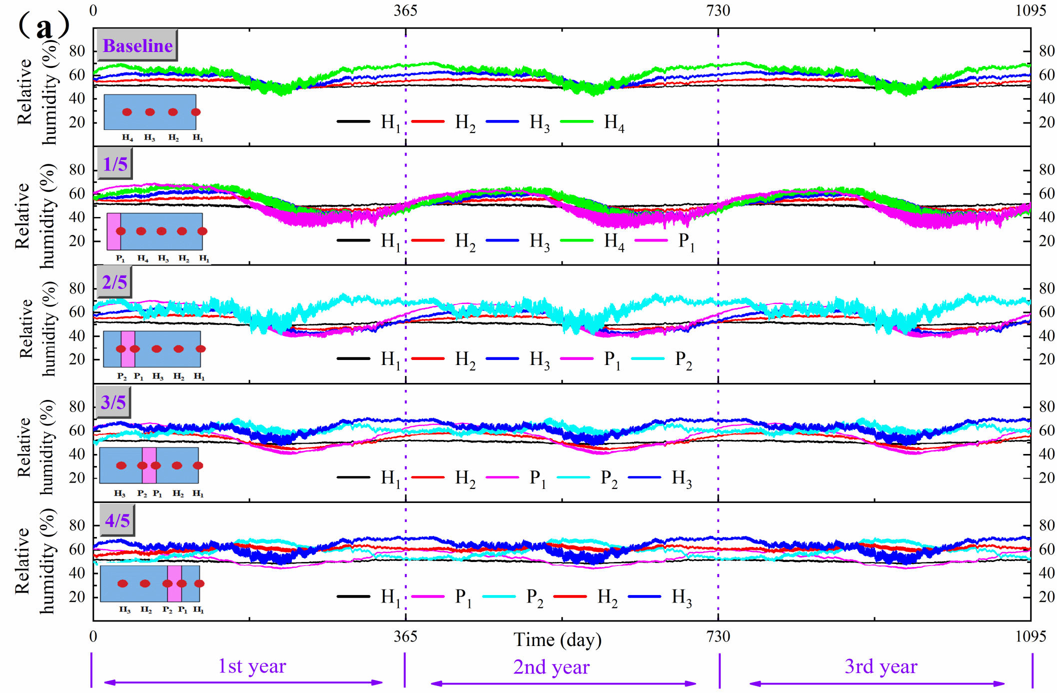

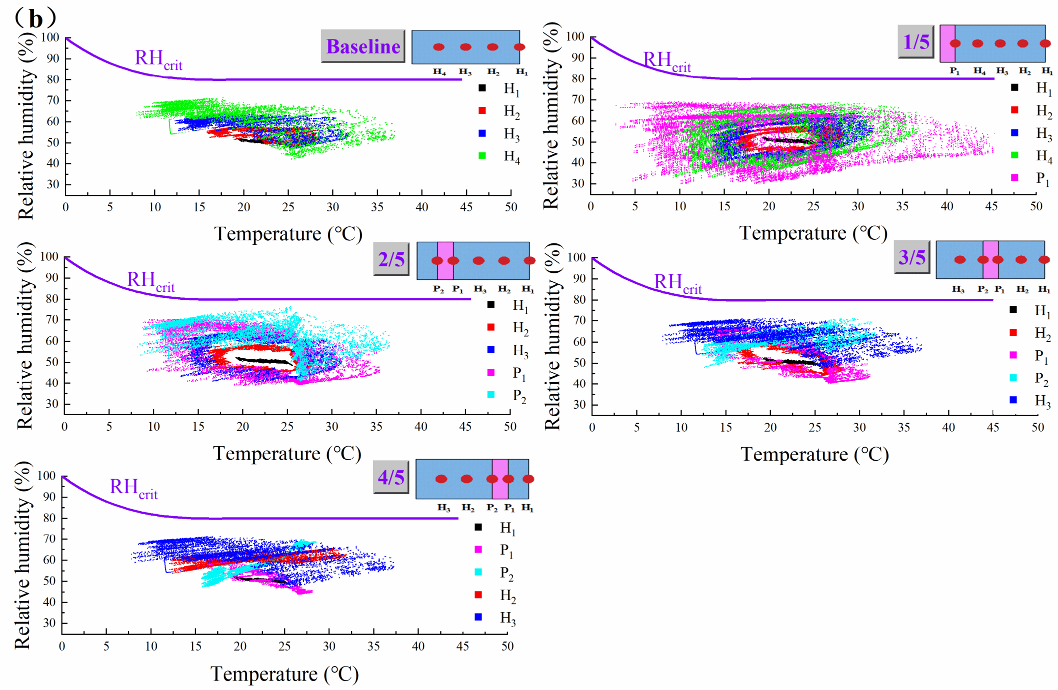

Fig. 15. Assessment of condensation and mold growth risk at various locations for different scenarios: (a) relative humidity variation; (b) temperature and relative humidity variations

6. Conclusion

In this study, PCM and bio-based concrete (i.e., HC) were integrated into a passive multilayer envelope. Four scenarios of the integrated envelope were proposed and compared to the baseline scenario. A simulation approach was used to study the energy and hygrothermal performance of the integrated envelope in Rome, Italy. The key findings and conclusions of the study are presented below.

The high coupling between moisture and heat transfer in the HC affects the energy and hygrothermal performance of the integrated envelope. On the one hand, temperature dominates the partial water vapor pressure and affects the variation of moisture flux/load, which affects the indoor thermal and hygric environment. On the other hand, moisture transfer is important for energy performance since the moisture load affects the latent heat load and thus the total heat load. Neglecting moisture transfer leads to an underestimation of annual heat load by 2.6% to 12.1% and of annual heat loss by 1.9% to 4.6%.

The energy and hygrothermal performance of the envelope can be optimized by changing the PCM location and properties. As the PCM moves toward the interior, the energy and hygrothermal performance improve. Thus, it is recommended to place the PCM close to the interior as the total heat load, temperature amplitude, and partial water vapor pressure amplitude are reduced by 8.2%, 46.3%, and 43.7%, respectively, in summer and 1.3%, 9.1%, and 8.2%, respectively, in winter, compared to the baseline scenario. Based on scenario 4/5, the reduction of heat load and of fluctuations in temperature and partial water vapor pressure are facilitated by increasing the thickness and latent heat as well as identifying the appropriate phase transition range (24–28 °C in summer and 16–20 °C in winter).

From a year-round perspective, the PCM reduces the heat gain in most scenarios compared to the baseline scenario, especially scenario 4/5, which showed the biggest annual heat gain reduction, 13.3%. In contrast, the PCM hardly affects annual heat loss. Moreover, scenario 4/5 is noteworthy in every season, as it saves energy and demonstrates adaptability in dealing with climatic relative humidity while guaranteeing moisture equilibrium within the HC.

The integrated envelope is free from the risk of condensation and mold growth. During the three-year assessment, the relative humidity at each location in each scenario showed a periodic variation with a one-year cycle and never exceeded 75%.

Overall, this work confirms the ability of the integrated envelope to improve the energy and hygrothermal performance of buildings and provides optimization strategies. The current work is a start, and future research aims to explore the economic feasibility of the integrated envelope by conducting an economic analysis.

CRediT authorship contribution statement

Dongxia Wu: Conceptualization, Methodology, Investigation, Data curation, Formal analysis, Writing - original draft. **Mourad Rahim:** Conceptualization, Methodology, Investigation, Formal analysis, Writing - review & editing. **Mohammed El Ganaoui:** Supervision, Project administration, Conceptualization, Methodology, Formal analysis, Writing - review & editing. **Rachid Bennacer:** Conceptualization, Methodology, Formal analysis, Writing - review & editing. **Bin Liu:** Methodology, Review & editing

Acknowledgements

We thank to the China Scholarship Council (CSC) for its financial support to the first author, No. 201808120084. CPER UL/Lorraine Region, PHC Maghreb, and EMPP Scientific Pole of the University of Lorraine are also acknowledged. I would also like to thank my wife, CF WANG, for her support of my research and care in my life.

Funding

This research did not receive any specific grant from funding agencies in the public, commercial, or not-for-profit sectors.

Appendix A

The equations of effective specific heat capacity and effective thermal conductivity as a function of temperature are as follows:

$$C^* = \begin{cases} C_S & T < T_{ini} \\ \frac{C_S + C_l}{2} + \beta \times exp\left(-1.67 \times \left(T - \frac{T_{ini}+T_{fin}}{2}\right)^2\right) & T_{ini} \ll T \ll T_{fin} \\ C_l & T > T_{fin} \end{cases}$$

(A.1)

$$\lambda^* = \begin{cases} \lambda_S & T < T_{ini} \\ \lambda_l + 0.01 \times (T_{fin} - T) & T_{ini} \ll T \ll T_{fin} \\ \lambda_l & T > T_{fin} \end{cases}$$

(A.2)

where T_{ini} and T_{fin} are the initial and final temperatures of the phase transition range, with their values listed in Table A.1; β is the coefficient that determines latent heat, with the relationship between β and latent heat shown in Table A.2; C_S and C_l are the specific heat capacities of solid and liquid PCM, $C_S = C_l = 2$ kJ/(kg·K); λ_S and λ_l are the thermal conductivities of solid and liquid PCM, $\lambda_S = 0.18$ W/(m·K) and $\lambda_l = 0.14$ W/(m·K).

Phase transition range	16–20 ℃	20–24 ℃	24–28 ℃	28–32 ℃
T_{ini} (℃)	16	20	24	28
T_{fin} (℃)	20	24	28	32

Table A.1 Initial and final temperature of different phase transition ranges

Latent heat of PCM (kJ/kg)	62.9	90.4	117.8	145.3
β	40	60	80	100

Table A.2 Relationship between β and latent heat of PCM

References

[1] G.A.f.B.a. Construction, 2020 Global status report for building and construction, 2020. https://wedocs.unep.org/bitstream/handle/20.500.11822/34572/GSR_ES.pdf. (accessed 04 December 2021).

[2] IEA, World Energy Outlook 2019, 2019. https://www.nordicenergy.org/wp-content/uploads/2019/12/6.2_12-Dec_14.00-14.30_WEOslides-for-DT-for-COP25-FINAL.pdf. (accessed 04 December 2021).

[3] L. Yang, J.-n. Huang, F. Zhou, Thermophysical properties and applications of nano-enhanced PCMs: An update review, Energy Conversion and Management 214 (2020) 112876.https://doi.org/10.1016/j.enconman.2020.112876

[4] D. Li, Y. Wu, C. Liu, G. Zhang, M. Arıcı, Energy investigation of glazed windows containing Nano-PCM in different seasons, Energy Conversion and Management 172 (2018) 119-128.https://doi.org/10.1016/j.enconman.2018.07.015

[5] M. Kabdrakhmanova, S.A. Memon, A. Saurbayeva, Implementation of the panel data regression analysis in PCM integrated buildings located in a humid subtropical climate, Energy 237 (2021) 121651.https://doi.org/10.1016/j.energy.2021.121651

[6] B. Larwa, S. Cesari, M. Bottarelli, Study on thermal performance of a PCM enhanced hydronic radiant floor heating system, Energy 225 (2021) 120245.https://doi.org/10.1016/j.energy.2021.120245

[7] S. Mousavi, B. Rismanchi, S. Brey, L. Aye, PCM embedded radiant chilled ceiling: A state-of-the-art review, Renewable and Sustainable Energy Reviews 151 (2021) 111601.https://doi.org/10.1016/j.rser.2021.111601

[8] A. Wieprzkowicz, D. Heim, Modelling of thermal processes in a glazing structure with temperature dependent optical properties - An example of PCM-window, Renewable Energy 160 (2020) 653-662.https://doi.org/10.1016/j.renene.2020.06.146

[9] P.K.S. Rathore, S.K. Shukla, Potential of macroencapsulated PCM for thermal energy storage in buildings: A comprehensive review, Construction and Building Materials 225 (2019) 723-

744.https://doi.org/10.1016/j.conbuildmat.2019.07.221

[10] K.O. Lee, M.A. Medina, E. Raith, X. Sun, Assessing the integration of a thin phase change material (PCM) layer in a residential building wall for heat transfer reduction and management, Applied Energy 137 (2015) 699-706.https://doi.org/10.1016/j.apenergy.2014.09.003

[11] Z.X. Li, A.A.A.A. Al-Rashed, M. Rostamzadeh, R. Kalbasi, A. Shahsavar, M. Afrand, Heat transfer reduction in buildings by embedding phase change material in multi-layer walls: Effects of repositioning, thermophysical properties and thickness of PCM, Energy Conversion and Management 195 (2019) 43-56.https://doi.org/10.1016/j.enconman.2019.04.075

[12] J. Yu, Q. Yang, H. Ye, Y. Luo, J. Huang, X. Xu, W. Gang, J. Wang, Thermal performance evaluation and optimal design of building roof with outer-layer shape-stabilized PCM, Renewable Energy 145 (2020) 2538-2549.https://doi.org/10.1016/j.renene.2019.08.026

[13] R.A. Kishore, M.V.A. Bianchi, C. Booten, J. Vidal, R. Jackson, Parametric and sensitivity analysis of a PCM-integrated wall for optimal thermal load modulation in lightweight buildings, Applied Thermal Engineering 187 (2021) 116568.https://doi.org/10.1016/j.applthermaleng.2021.116568

[14] M.h. Dehmous, E. Franquet, N. Lamrous, Mechanical and thermal characterizations of various thermal energy storage concretes including low-cost bio-sourced PCM, Energy and Buildings 241 (2021) 110878.https://doi.org/10.1016/j.enbuild.2021.110878

[15] Y. Florentin, D. Pearlmutter, B. Givoni, E. Gal, A life-cycle energy and carbon analysis of hemp-lime bio-composite building materials, Energy and Buildings 156 (2017) 293-305.https://doi.org/10.1016/j.enbuild.2017.09.097

[16] M. Dlimi, O. Iken, R. Agounoun, A. Zoubir, I. Kadiri, K. Sbai, Energy performance and thickness optimization of hemp wool insulation and air cavity layers integrated in Moroccan building walls', Sustainable Production and Consumption 20 (2019) 273-288.https://doi.org/10.1016/j.spc.2019.07.008

[17] N. Chennouf, B. Agoudjil, A. Boudenne, K. Benzarti, F. Bouras, Hygrothermal characterization of a new bio-based construction material: Concrete reinforced with date palm fibers, Construction and Building Materials 192 (2018) 348-356.https://doi.org/10.1016/j.conbuildmat.2018.10.089

[18] M. Rahim, O. Douzane, A.D. Tran Le, G. Promis, B. Laidoudi, A. Crigny, B. Dupre, T. Langlet, Characterization of flax lime and hemp lime concretes: Hygric properties and moisture buffer capacity, Energy and Buildings 88 (2015) 91-99.https://doi.org/10.1016/j.enbuild.2014.11.043

[19] S. Poyet, S. Charles, Temperature dependence of the sorption isotherms of cement-based materials: Heat of sorption and Clausius–Clapeyron formula, Cement and Concrete Research 39(11) (2009) 1060-1067.https://doi.org/10.1016/j.cemconres.2009.07.018

[20] N. Chennouf, B. Agoudjil, T. Alioua, A. Boudenne, K. Benzarti, Experimental investigation on hygrothermal performance of a bio-based wall made of cement mortar filled with date palm fibers, Energy and Buildings 202 (2019) 109413.https://doi.org/10.1016/j.enbuild.2019.109413

[21] D. Wu, M. Rahim, M. El Ganaoui, R. Djedjig, R. Bennacer, B. Liu, Experimental investigation on the hygrothermal behavior of a new multilayer building envelope integrating PCM with bio-based material, Building and Environment 201 (2021) 107995.https://doi.org/10.1016/j.buildenv.2021.107995

[22] T. Colinart, P. Glouannec, M. Bendouma, P. Chauvelon, Temperature dependence of sorption isotherm of hygroscopic building materials. Part 2: Influence on hygrothermal behavior of hemp concrete, Energy and Buildings 152 (2017) 42-51.https://doi.org/10.1016/j.enbuild.2017.07.016

[23] X. He, H. Zhang, L. Qiu, Z. Mao, C. Shi, Hygrothermal performance of temperature-humidity controlling materials

with different compositions, Energy and Buildings 236 (2021) 110792.https://doi.org/10.1016/j.enbuild.2021.110792

[24] Z. Chen, M. Qin, Preparation and hygrothermal properties of composite phase change humidity control materials, Applied Thermal Engineering 98 (2016) 1150-1157.https://doi.org/10.1016/j.applthermaleng.2015.12.096

[25] A. Oliver, Thermal characterization of gypsum boards with PCM included: Thermal energy storage in buildings through latent heat, Energy and Buildings 48 (2012) 1-7.https://doi.org/10.1016/j.enbuild.2012.01.026

[26] P. Hou, M. Qin, S. Cui, K. Zu, Preparation and characterization of metal-organic framework /microencapsulated phase change material composites for indoor hygrothermal control, Journal of Building Engineering 31 (2020) 101345.https://doi.org/10.1016/j.jobe.2020.101345

[27] Z. Wu, M. Qin, Z. Chen, Phase Change Humidity Control Material and its Application in Buildings, Procedia Engineering 205 (2017) 1011-1018.https://doi.org/10.1016/j.proeng.2017.10.162

[28] Y. Fraine, C. Seladji, A. Aït-Mokhtar, Effect of microencapsulation phase change material and diatomite composite filling on hygrothermal performance of sintered hollow bricks, Building and Environment 154 (2019) 145-154.https://doi.org/10.1016/j.buildenv.2019.02.036

[29] X. Shi, S.A. Memon, W. Tang, H. Cui, F. Xing, Experimental assessment of position of macro encapsulated phase change material in concrete walls on indoor temperatures and humidity levels, Energy and Buildings 71 (2014) 80-87.https://doi.org/10.1016/j.enbuild.2013.12.001

[30] J.H. Park, Y. Kang, J. Lee, S. Wi, J.D. Chang, S. Kim, Analysis of walls of functional gypsum board added with porous material and phase change material to improve hygrothermal performance, Energy and Buildings 183 (2019) 803-816.https://doi.org/10.1016/j.enbuild.2018.11.023

[31] S.J. Chang, Y. Kang, S. Wi, S.-G. Jeong, S. Kim, Hygrothermal performance improvement of the Korean wood frame walls using macro-packed phase change materials (MPPCM), Applied Thermal Engineering 114 (2017) 457-465.https://doi.org/10.1016/j.applthermaleng.2016.11.188

[32] Z. Wu, M. Qin, M. Zhang, Phase change humidity control material and its impact on building energy consumption, Energy and Buildings 174 (2018) 254-261.https://doi.org/10.1016/j.enbuild.2018.06.036

[33] C. Piselli, M. Prabhakar, A. de Gracia, M. Saffari, A.L. Pisello, L.F. Cabeza, Optimal control of natural ventilation as passive cooling strategy for improving the energy performance of building envelope with PCM integration, Renewable Energy 162 (2020) 171-181.https://doi.org/10.1016/j.renene.2020.07.043

[34] F. Benmahiddine, F. Bennai, R. Cherif, R. Belarbi, A. Tahakourt, K. Abahri, Experimental investigation on the influence of immersion/drying cycles on the hygrothermal and mechanical properties of hemp concrete, Journal of Building Engineering 32 (2020) 101758.https://doi.org/10.1016/j.jobe.2020.101758

[35] D. Energain®, Hydrocarbon-based PCM Applications, 2010. https://cdn2.hubspot.net/hub/55819/file-14755587-pdf/docs/buildings-xi/dupont_energain.pdf. (accessed 04 December 2021).

[36] M. Rahim, A.D. Tran Le, O. Douzane, G. Promis, T. Langlet, Numerical investigation of the effect of non-isotherme sorption characteristics on hygrothermal behavior of two bio-based building walls, Journal of Building Engineering 7 (2016) 263-272.https://doi.org/10.1016/j.jobe.2016.07.003

[37] A. Fick, Ueber Diffusion, 170(1) (1855) 59-86.10.1002/andp.18551700105

[38] S. Whitaker, Flow in porous media I: A theoretical derivation of Darcy's law, Transport in Porous Media 1(1) (1986) 3-25.10.1007/BF01036523

[39] H.M.J.F.I.o.b.p. Kunzel, Allemagne, Simultaneous heat and moisture transport in building components, (1995)

[40] T. Colinart, P. Glouannec, Temperature dependence of sorption isotherm of hygroscopic building materials. Part 1: Experimental evidence and modeling, Energy and Buildings 139 (2017) 360-

370.https://doi.org/10.1016/j.enbuild.2016.12.082

[41] R. Peuhkuri, Moisture Dynamics in Building Envelopes, (2003)

[42] K.P. Galvin, A conceptually simple derivation of the Kelvin equation, Chemical Engineering Science 60(16) (2005) 4659-4660.https://doi.org/10.1016/j.ces.2005.03.030

[43] Y. Wang, Y. Fan, D. Wang, Y. Liu, J. Liu, The effect of moisture transfer on the inner surface thermal performance and the thermal transmittance of the roof-wall corner building node in high-temperature and high-humidity areas, Journal of Building Engineering 44 (2021) 102949.https://doi.org/10.1016/j.jobe.2021.102949

[44] N. Mendes, P.C. Philippi, R. Lamberts, A new mathematical method to solve highly coupled equations of heat and mass transfer in porous media, International Journal of Heat and Mass Transfer 45(3) (2002) 509-518.https://doi.org/10.1016/S0017-9310(01)00172-7

[45] S. Zhou, R. Zhang, Z. Zhang, Climatology and meteorology, (2002)

[46] S. Wijesuriya, P.C. Tabares-Velasco, K. Biswas, D. Heim, Empirical validation and comparison of PCM modeling algorithms commonly used in building energy and hygrothermal software, Building and Environment 173 (2020) 106750.https://doi.org/10.1016/j.buildenv.2020.106750

[47] L.P. Li, Z.G. Wu, Y.L. He, G. Lauriat, W.Q. Tao, Optimization of the configuration of 290×140×90 hollow clay bricks with 3-D numerical simulation by finite volume method, Energy and Buildings 40(10) (2008) 1790-1798.https://doi.org/10.1016/j.enbuild.2008.03.010

[48] G.N. Walton, Thermal Analysis Research Program Reference Manual, National Bureau of Standards, March (1983).https://doi.org/10.1016/j.jobe.2016.07.003

[49] W.C. Swinbank, Long-wave radiation from clear skies, Quarterly Journal of the Royal Meteorological Society 89(381) (1963) 339-348.https://doi.org/10.1002/qj.49708938105

[50] C. Rode, R. Peuhkuri, H. Lone, B. Time, A. Gustavsen, T. Ojanen, J. Ahonen, K. Svennberg, L.-E. Harderup, J. Arfvidsson, Moisture buffering of building materials, (2006)

[51] M. Kottek, J. Grieser, C. Beck, B. Rudolf, F. Rubel, World map of the Köppen-Geiger climate classification updated, (2006).https://doi.org/10.1127/0941-2948/2006/0130

[52] E.I. 13788:, Hygrothermal performance of building components and building elements–internal surface temperature to avoid critical surface humidity and interstitial condensation–calculation methods (European Committee for Standardization), (2012)

[53] P.W. O'Callaghan, S.D. Probert, Sol-air temperature, Applied Energy 3(4) (1977) 307-311.https://doi.org/10.1016/0306-2619(77)90017-4

[54] A.J.A.S.o.H. Standard, Refrigerating, I. Air-Conditioning Engineers, Criteria for Moisture-Control Design Analysis in Buildings, (2009)

[55] A. Hukka, H.A. Viitanen, A mathematical model of mould growth on wooden material, Wood Science and Technology 33(6) (1999) 475-485.https://doi.org/10.1007/s002260050131

[56] A. Fateh, F. Klinker, M. Brütting, H. Weinläder, F. Devia, Numerical and experimental investigation of an insulation layer with phase change materials (PCMs), Energy and Buildings 153 (2017) 231-240.https://doi.org/10.1016/j.enbuild.2017.08.007

[57] R.A. Kishore, M.V.A. Bianchi, C. Booten, J. Vidal, R. Jackson, Optimizing PCM-integrated walls for potential energy savings in U.S. Buildings, Energy and Buildings 226 (2020) 110355.https://doi.org/10.1016/j.enbuild.2020.110355

[58] D.A. Neeper, Thermal dynamics of wallboard with latent heat storage, Solar Energy 68(5) (2000) 393-

403.https://doi.org/10.1016/S0038-092X(00)00012-8

[59] K. Biswas, R. Abhari, Low-cost phase change material as an energy storage medium in building envelopes: Experimental and numerical analyses, Energy Conversion and Management 88 (2014) 1020-1031.https://doi.org/10.1016/j.enconman.2014.09.003